CH9300597

LRP 480/93 . July 1993

ACTIVE FEEDBACK STABILIZATION OF AXISYMMETRIC MODES IN HIGHLY ELONGATED TOKAMAK PLASMAS

D.J. Ward and F. Hofmann

C R P P

ÉCOLE POLYTECHNIQUE FÉDÉRALE DE LAUSANNE - SUISSE

LRP 480/93 July 1993

ACTIVE FEEDBACK STABILIZATION OF AXISYMMETRIC MODES IN HIGHLY ELONGATED TOKAMAK PLASMAS

D.J. Ward and F. Hofmann

Active Feedback Stabilization of Axisymmetric Modes in Highly Elongated Tokamak Plasmas

D. J. Ward and F. Hofmann
Centre de Recherches en Physique des Plasmas,
Association Euratom–Confédération Suisse,
Ecole Polytechnique Fédérale de Lausanne,
21 av. des Bains, 1007 Lausanne, Switzerland

Abstract

Active feedback stabilization of the vertical instability is studied for highly elongated tokamak plasmas ($2 \leq \kappa \leq 3$), and evaluated in particular for the TCV configuration. It is shown that the feedback can strongly affect the form of the eigenfunction for these highly elongated equilibria, and this can have detrimental effects on the ability of the feedback system to properly detect and stabilize the plasma. A calculation of the vertical displacement that uses poloidal flux measurements, poloidal magnetic field measurements, and corrections for the vessel eddy currents and active feedback currents was found to be effective even in the cases with the worst deformations of the eigenfunction. We also examine how these deformations affect differently shaped equilibria, and it is seen that the magnitude of the deformation of the eigenfunction is a strong function of the plasma elongation.

1. Introduction

Elongation and shaping of the plasma cross section has long been understood to be a way to achieve improved beta limits and confinement in tokamaks [1,2]. Experimental results have shown that obtainable beta values can be significantly increased by the optimization of plasma shape [3]. However, highly shaped tokamaks are plagued by a dangerous vertical, or axisymmetric, instability. Therefore, the feedback stabilization of this instability in tokamaks has been the object of considerable study [4–8].

It has been shown [7,8] that elongated plasmas being stabilized against the vertical instability by feedback will have eigenfunctions that are modified to minimize the energy of the system of the plasma and feedback together. These modifications in the eigenfunction are such that the effectiveness of the feedback system is reduced. In the case of passive feedback by a set of conductors [8] it was seen that the eigenfunction of the partially stabilized plasma was modified such that the eddy currents in the given set of conductors were reduced, compared to those that would result form the original form of the eigenfunction (with no wall or a uniform wall). This is especially important for conductors localized in one area near the plasma. If the conductors are moved to another location the eigenfunction will again be modified to reduce the stabilizing eddy currents in that conductor configuration. In the case of active feedback [7,8] it was shown that the eigenfunction could be modified such that the perturbed flux signal at the location of the detectors for the feedback system was reduced. If the flux-loops were moved it was seen that the eigenfunction would be modified in a different way, which again would reduce the signal. In some cases, this could happen to such an extent that the signal was reduced to be insignificant, and the feedback system was rendered ineffective.

We shall see that highly elongated equilibria are subject to the same deformations of the eigenfunction with respect to the detector position, as described above, but also to a deformation of the eigenfunction, which is induced by the particular active feedback

coil configuration. These types of deformations are most often insensitive to the positions of the magnetic detectors, but rather are determined by the arrangement of the active feedback coils. However, these deformations can have a strong effect on the ability of the magnetic detectors to effectively measure vertical displacement as part of a feedback system. We will see that in these highly elongated tokamak equilibria the eigenfunction can be modified to such an extent that it is no longer dominated at the plasma edge by the $m = 1$ component, but instead by a higher-m component. This does not necessarily reduce the ability of the active coil set to stabilize the plasma, but it can make the detection system ineffective, depending on the nature of the magnetic measurements and the deformation of the eigenfunction.

In this paper we study the active feedback of highly elongated plasmas ($2 \leq \kappa \leq 3$) in the TCV [9] design configuration. We perform these calculations using the NOVA-W code [10]. NOVA-W is a linear MHD stability code which includes resistive conductors and an active feedback system in the vacuum calculation. The NOVA-W code has recently been improved to include several new features in the calculation: active feedback coils inside the vacuum vessel, an arbitrary combination of multiple poloidal flux and poloidal magnetic field (B_p) measurements, plus corrections due to active coil currents and vessel eddy currents to give the magnetic measurement of vertical displacement. These features are necessary in order to perform general studies of the TCV vertical feedback control system. We shall demonstrate that a calculation of the vertical displacement that uses a combination of these measurements and corrections is effective in spite of large deformations of the eigenfunction.

This paper is organized as follows. The following section describes the TCV vertical feedback configuration and the equilibrium used in this study. Section 3 describes the deformable plasma results using the TCV configuration. Cases are presented showing how the deformability can depend on detector position, but it is seen that the configuration of active coils determines the deformation in most cases. In Section 4 we show how the

deformable plasma effects are a function of the plasma shape, and how they are much less significant for equilibria of more moderate shape than for the fully elongated TCV plasmas. In Section 5 we conclude and summarize our results.

2. The TCV Configuration

Figure 1 shows a cross-section of the TCV vacuum vessel, active feedback coils, flux loops and B_p coils, and the fully elongated TCV equilibrium used in this study. Also shown are the contours of perturbed plasma flux for this equilibrium without active feedback. This equilibrium, which we will use throughout Section 3, is a standard "TCV dee" equilibrium. The shape of the plasma-vacuum boundary [11] is described by:

$$R/a = A + \cos(\theta + \delta \sin\theta + \lambda \sin 2\theta) \quad , \quad Z/a = \kappa \sin\theta \tag{1}$$

The TCV dee shape has $A = 3.67$, $\kappa = 3$, $\delta = 0.5$, $\lambda = 0.2$, and $a = 0.24$ m. Here, A is the aspect ratio, κ is the elongation, δ is the triangularity, and λ is a squareness parameter that modifies the shape of the tips, e.g., $\lambda > 0$ makes the tips broader. The equilibrium has an internal inductance given by $l_i = 0.53$, where

$$l_i \equiv \frac{2}{\mu_0^2 I_p^2 R_0} \int_V B_p^2 d^3x \tag{2}$$

Using the G.A. definition, this equilibrium has $l_i(\text{G.A.}) = 0.82$, where

$$l_i(\text{G.A.}) \equiv \frac{(\oint_S dl)^2 \int_V B_p^2 d^3x}{(V \oint_S B_p dl)^2} \tag{3}$$

This particular equilibrium has a growth rate in the absence of active feedback (and without the additional passive stabilization from the internal coils) of $\gamma \approx 2100$ s^{-1}. This is quite close to the the maximum growth rate which we believe can be stabilized using the TCV feedback system. (The time constant for the $m = 1$ eigenmode of the TCV vacuum vessel is approximately 8 ms.)

TCV has 2 active feedback coils inside the vacuum vessel and 16 active coils outside the vessel. The two internal coils are driven by a fast power supply with a response time on the order of 0.2 ms. The external coils have power supplies which respond on a slower (1 ms) time scale, but are more powerful, so that they will provide the long term stabilization. The external feedback coils are all independent and may be used in any combination with arbitrarily weighted voltage.

We use a two-time-scale feedback system [12] using both the internal and external active coils. The voltage applied to the internal coils is equal to some gain (proportional plus derivative) multiplied by a measure of the vertical displacement, δZ, which is composed of a combination of perturbed flux and B_p measurements. The voltage applied to the external coils is proportional to the current in the internal coils. Thus,

$$V_j^{i.c.} = \alpha_j \delta Z + \beta_j \delta \dot{Z} \tag{4}$$

$$V_k^{e.c} = G_{kj} I_j^{i.c.} \tag{5}$$

The internal coils provide the fast response necessary to stabilize these highly elongated plasmas, but they have power limitations, so this two stage system allows the current in the fast internal coils to return to zero by replacing their stabilizing force by that of the more powerful, but slower, external coils.

One can also define a second level of feedback [12] in which a *desired* current in a feedback coil is defined

$$I_i^{des} = \tilde{\alpha}_i \delta Z + \tilde{\beta}_i \delta \dot{Z} \tag{6}$$

and the necessary voltage applied to the coil is given by

$$V_i = G_i (I_i^{des} - I_i), \tag{7}$$

where I_i is the actual coil current. However, for most of the calculations in this paper we will use active feedback as defined by Eqs. (4) and (5).

We are considering here the problem of the deformation of the eigenfunction induced by the active feedback system, and the effectiveness of the magnetic detection system in such cases. Therefore, we will not perform a detailed study of the optimization of the gains in Eqs. (4) and (5). We keep the ratio of β_j/α_j fixed at 0.02 s and $G_{kj} = 0.0025 V_k^w$ V/A for all the cases considered here, where V_k^w is a weighting factor that may vary for the different external coils.

The magnetics measurements are composed of a combination of poloidal flux measurements from 38 flux loops just outside the resistive wall (shown in Fig. 1 by an 'X') and poloidal field measurements from 38 B_p-coils just inside the vacuum vessel wall (each is marked by a 'c'). These measurements are combined in a weighted sum [13] to determine the vertical displacement δZ:

$$I_p \delta Z = \sum_i a_i \delta\psi_i + \sum_j b_j \delta B_j + \sum_k c_k \delta I_k + \sum_l d_l \delta\dot{\psi}_l \tag{8}$$

where $\delta\psi_i$ are the perturbed flux measurements, δB_j are the poloidal field measurements, δI_k are the active feedback coil currents, and the terms $d_l \delta\dot{\psi}_l$ account for the effect of the eddy currents in the lth vessel element.

We consider detection systems ranging from a single pair of flux loops and/or B_p-coils (without corrections from coil currents) to the full combination of measurements of Eq. (8). Here we reference the flux-loop, B_p-coil pairs (which are up-down symmetric about the midplane) from #1 at the inboard midplane to #20 at the outboard midplane. The numbering sequence is shown in Fig. 1.

3. Deformable Plasma Effects

The NOVA-W code decomposes the plasma displacement such that the eigenfunction is represented by a sum over the poloidal harmonics:

$$\xi_\psi = \vec{\xi} \cdot \nabla\psi = \sum_m \xi_{\psi m} \exp(im\Theta). \tag{9}$$

Here, ψ is the poloidal flux, Θ is the poloidal angular variable corresponding to the equal-arc-length, straight-field-line coordinate system. When we talk of deformations of the eigenfunction, we refer to variations in the poloidal harmonics $\xi_{\psi m}$. In particular, we usually plot the ratio of the m^{th} harmonic to the $m = 1$ harmonic, $\xi_{\psi m}/\xi_{\psi 1}$, at the plasma edge, as a simple way to illustrate the changes in the eigenfunction due to the influence of the feedback system.

3.1. Deformation of the Eigenfunction Determined by Detector Configuration

We first consider a case that demonstrates the effect described in Ref. [8], i.e., the modification of the eigenfunction of a plasma undergoing active feedback stabilization when the magnetic detectors are moved. We consider the $\kappa = 3$ TCV dee equilibrium described above, and we use an active feedback system consisting of only two active coils external to the vacuum vessel and on the outboard side located at $(X, Z) = (1.30, \pm 0.775)$. The vertical displacement is detected by the flux difference of a single pair of flux loops, which are symmetric about the midplane. We move the flux loops slightly to see how the behavior changes.

Figure 2 shows the configuration with the two different sets of flux loops. Shown are the contours of zero-flux at three different values of gain (dot-dash, dashed, dotted, respectively, with increasing gain) for the two configurations. In the case shown in Fig. 2a—flux loops located at $(X, Z) = (0.60, \pm 0.772)$—we see that the zero-flux contours approach the flux loops as the gain is increased, thereby making them ineffective. Figures 3a and 3b show the evolution of the different components of the eigenfunction with increasing gain for the case where the flux loops are located as in Fig. 2a. We see that there is a sharp reversal in the evolution of the components $\xi_{\psi m}/\xi_{\psi 1}$ with respect to gain in Fig. 3. This point corresponds to the stage in the evolution where the zero-flux contour begins to move towards the flux

loops in Fig. 2a.

In Fig. 2b we see the difference in the behavior when the flux loops are moved just 8 cm towards the midplane, to the new location at $(X, Z) = (0.584, \pm 0.690)$. The zero-flux contours in Fig. 2b move continuously away from the flux loops with increasing gain—compare this to the behavior of Fig. 2a where the eigenfunction changes such that the zero-flux contours move towards the flux loops. Figures 4a and 4b show the evolution of the different poloidal harmonics of the eigenfunction and the growth rate for this second case. We see that the eigenfunction evolves in a completely different way from the first case.

Also plotted in Figs. 3a and 4a is the normalized, measured signal at the flux loops $\delta\chi$ for the two cases. In Fig. 3a we see that the perturbed flux signal reaches a maximum and then decreases. Eventually the signal decreases at the same rate that the gain increases. From this point onward the growth rate γ stays constant because the feedback system is unable to further stabilize the instability. The point at which the perturbed flux signal begins to decrease corresponds to the point where the components $\xi_{\psi m}/\xi_{\psi 1}$ of the eigenfunction begin to undergo a sudden and rapid change. Clearly, in this case, there is a strong modification of the eigenfunction which reduces the measurable flux signal at the flux loops.

Figure 4a shows a completely different evolution in the perturbed flux signal. It increases, then levels off somewhat, but continues to increase slowly. The flux loops are adequate to measure the signal in this case. Even though we see that the eigenfunction in Fig. 4 is strongly modified with increasing gain, it does not cause a limitation of the measured signal. Also, the evolution of the eigenfunction shown in Fig. 4 is not affected by moving the flux loops further towards the midplane on the inboard side. Apparently, with the flux loops at these locations, it is no longer energetically favorable for the eigenfunction to undergo a strong modification that would reduce the measurable flux signal at the flux loops as in the first case. However, the eigenfunction is seen in Fig. 4 to be undergoing a very strong modification, but one that does not reduce the flux signal—in fact, the flux

signal increases steadily. It is interesting to remember that this impressive difference in the behavior of the eigenfunction for these two cases is due to a movement of the flux-loop position by only 8 cm.

3.2. *Deformation of the Eigenfunction Determined by Active Coil Configuration*

3.2.1. *Active feedback using a small number of coils*

We show here that the configuration of, and the weighting of currents in, the active feedback coils can induce a particular deformation in the eigenfunction. For a system with active coils that are not far away from the plasma compared to the magnetic detectors, we see that the deformation is not a sensitive function of the detectors' position. This deformation is not necessarily detrimental, but, depending on the configuration of magnetic detectors used by the feedback system, it can have a serious effect on the ability of the feedback system to stabilize the plasma.

Let us first reconsider the case shown in Fig. 4, which shows a very large deformation of the eigenfunction, but no reduction in the flux signal. We see from Fig. 4 that the eigenfunction is modified such that the $m = 2$ component changes sign and then grows in magnitude until it dominates the $m = 1$ component at the plasma edge. Figure 5 shows the complete set of perturbed flux contours for this case at the marginally unstable point. The $m = 2$ component at the edge is about -1.27 times the $m = 1$ component at this gain value. The perturbed flux contour plot shows a large deformation that bulges towards the inboard side and the zero-flux contour in contact with the plasma boundary. This deformation in the perturbed flux reflects the $m = 2$ dominance of the modified eigenfunction. Comparing Fig. 5 to Fig. 1 (no feedback) one sees that the character of the instability is completely different from the passive case.

If the active feedback coils are moved from the outboard side to the inboard side (see Fig. 1), and the flux loops are moved correspondingly from the inboard to the outboard side, the deformation of the eigenfunction with increasing gain behaves similarly, but the sign of the $m = 2$ component is opposite. In other words, $\xi_{\psi 2}/\xi_{\psi 1}$ remains positive and increases in magnitude to values of roughly equal magnitude as in Fig. 4. Likewise, the plot of perturbed flux contours shows a deformation in which the flux bulges to the outboard side, but with the same $m = 2$ character as in Fig. 5.

As a second case let us consider a feedback system using two pairs of active coils—one pair inside the vessel on the outboard side and one pair outside the vessel on the inboard side. We use the feedback law described in Eqs. (4) and (5). The configuration of coils and detectors is shown in Fig. 7. (Note that if we use the internal coils and a single pair of external coils on the *outboard* side we get behavior quite similar to that shown in Figs. 4 and 5.)

Figure 6 shows the evolution of the various poloidal harmonics of the eigenfunction with respect to increasing gain. We see that in this case the largest variation is in the $m = 3$ component. This component increases greatly in magnitude until it dominates at the edge. The $m = 2$ and $m = 4$ components vary slightly, but their variation is relatively small compared to that of the $m = 3$ component.

Figure 7 shows the contours of perturbed flux for this case. The deformation of the eigenfunction in comparison to Figs. 1 and 5 is clear. It shows the domination of the $m = 3$ component to the eigenfunction by the outward deformation in the perturbed flux on the inboard and outboard sides and the inward deformation at the top and bottom.

These large deformations of the eigenfunction, such that it becomes dominated by $m = 2$ or $m = 3$ harmonics, do not necessarily keep the feedback system from stabilizing the plasma. Figures 4 and 6 show that the plasma is indeed stabilized using this combination of active coils and flux loops.

3.2.2. *Active feedback using the full set of coils*

Next we consider a feedback system where we use all the available active feedback coils. The internal and external coils are used together as described in Eqs. (4) and (5), and the external coils are all given equal voltage weighting. If we use the complete magnetic detection system with corrections described in Eq. (8), the plasma is easily stabilized with this feedback system, since the total magnetic signal is nearly unaffected by the deformation. Because of the uniform weighting of the coil voltages, there is not any dominance, nor any large variation, of a particular component of the eigenfunction for this case.

Nevertheless, there is a clear deformation induced by the active coils in this case which is illustrated by the plot of the perturbed flux contours in Fig. 8. There is a characteristic deformation of the perturbed flux, which is seen by comparing Figs. 1 and 8, whereby there is an indentation near the internal coils, and consequently there is a slight outward bulge in the perturbed flux contours on the outboard side between the internal coils and the midplane. There is also a large bulge in the perturbed flux contours at the top and bottom of the plasma.

It is apparent from the fact that the zero-flux contour in Fig. 8 lies so close to most of the flux loops that most pairs of flux loops if used by themselves would be ineffective. An example of an *effective* single pair of flux loops is pair #17, because the outboard bulge of the perturbed flux increases the measurable signal at the nearby flux loops. We find that the evolution of the eigenfunction and the growth rate vs. the normalized gain due to active feedback is virtually the same when flux-loop pair #17 is alone used as when the complete set of flux-loop and B_p-coil measurements is used for this case. In this case one could take advantage of the deformation in the eigenfunction due to the influence of the internal coils to use flux loops that would be quite ineffective without this deformation. The flux-loop pairs that are effective when used by themselves are at positions #10, #11, #17, #18, and #19.

If the measurement from the corresponding pair of B_p-coils is added to the measurement from a single pair of the flux loops, the combination is effective for *most* of the pairs. However this is not true in all cases, and one must still be careful in choosing the location of the flux-loop, B_p-coil pairs. In some cases the sum of a negative flux measurement plus a positive B_p measurement yields a null signal. The *ineffective* locations for the flux-loop, B_p-coil pairs are at positions #7, #8, #9, #12, #13, #14, and #15.

Next we consider a different weighting of the active feedback coil set. The voltage weights on the external coils are weighted in proportion to the vertical distance from the midplane, and the outboard coils are given a stronger weight compared to those on the inboard side by a factor of about 3.5. This results in the active feedback coils generating a more uniform raidal field inside the vacuum vessel than in the previous case.

The variation of the poloidal harmonics, growth rate, and measured signal are shown in Figs. 9a and 9b. Because of the weighting of voltages of the feedback coils in this case, there is a significant deformation of the plasma eigenfunction. In particular, there is a sharp drop in $\xi_{\psi 2}/\xi_{\psi 1}$ beginning at a normalized gain value of about 4×10^{-5}. Examination of the normalized signal, however, shows that this deformation has little effect on the measured, corrected signal $|\delta Z|$ and therefore stabilization is achieved. Figure 10 shows the perturbed flux contours at the marginal stability point for this configuration. It can be seen that if only a single pair of flux loops or flux-loop, B_p-coil combination (without corrections) is used then most detectors on the outboard side would be ineffective, while most on the inboard side would be reasonably effective.

Clearly, one really desires a combination of magnetic measurements that is effective independent of the equilibrium and the details of the weighting of the currents in the active coils. For this reason we propose to use a combination of poloidal flux and poloidal field measurements, plus corrections due to active coil currents and vessel eddy currents as in Eq. (8). This has been found to be completely effective for all active feedback configurations tested so far in spite of the large deformations of the eigenfunction that sometimes occur.

4. Effect of Plasma Shape on Deformability

It is clear that in the most highly elongated ($\kappa = 3$) TCV equilibria the active feedback system can induce large deformations in the eigenfunction. We will consider how the eigenfunction is affected by active feedback in equilibria with more moderate shaping. We will see that these deformations are still present in the eigenfunction at lower elongation, but that these deformations become less significant as the elongation is reduced. One also sees that the deformation couples to other harmonics for the case with the highest elongation ($\kappa = 3$), but that this coupling is greatly reduced at lower elongation.

As we are now considering the relation between the deformability and the plasma shape, we would like to keep the relation between the equilibrium shape and the feedback system as consistent as possible. Therefore, we will not use the TCV wall and coil configuration as in Section 3. But rather we will use a resistive wall for each equilibrium which is a function of the plasma shape, and the position of the active coils will also be chosen as a function of the shape.

In particular, the shape of the resistive wall is taken to be that of the plasma surface, but with the minor radius increased by some factor. We consider equilibria at four elongations, $\kappa = 1.75, 2.0, 2.5, 3.0$. For the $\kappa = 3$ equilibrium we have a wall expanded by a factor of 1.2 from the plasma surface. Since we are considering the variation in the eigenfunction vs. the eigenvalue, or growth rate, we want the passive growth rate (i.e., no active feedback) to have the same value for all three cases. Therefore we adjust the expansion factor of the resistive wall for the cases with $\kappa < 3$, so that they have the same passive growth rate. As is turns out, the degree of deformation is not a strong function of the passive growth rate, and thus the deformation of the eigenfunction under active feedback is nearly identical for the different resistive wall distances.

4.1. *Active Feedback Induced $m = 2$ Deformation*

First we consider a case with a single pair of active feedback coils on the outboard side at $X = 1.20$ m, whose vertical positions are such that the coils are level with the top and bottom of the plasma. The flux loops are placed in an effective position, where their location was chosen to have no effect on the deformation of the eigenfunction. This is similar to the case described in Fig. 4. In that case it was seen that there was a very large enhancement of the $m = 2$ component by the feedback system.

We use the generic prescription for the resistive wall and the active coil placement as discussed above, and compare the evolution of the $m = 2$ and $m = 3$ harmonics for these four equilibria of differing elongation. Figure 11a shows the evolution of ratio $\xi_{\psi 2}/\xi_{\psi 1}$ vs. γ_τ for the four cases, and Fig. 11b shows the same evolution for $\xi_{\psi 3}/\xi_{\psi 1}$. We plot these quantities vs. growth rate because this gives the best comparison of the harmonics of the eigenfunction with different amounts of stabilization. Therefore the direction of increasing gain is towards the left, i.e. towards reduced growth rate. Recall that the wall is adjusted so that all cases have the same passive growth rate.

We see in Fig. 11a that there is a significant enhancement in the $m = 2$ component for the highly elongated plasmas. For the $\kappa = 3$ case the $m = 2$ component near the edge is larger than the $m = 1$ component by a factor of 2. For the $\kappa = 2.5$ case this enhancement is smaller, but the eigenfunction at the edge is still dominated by the $m = 2$ harmonic. For the $\kappa = 2$ case there is still clearly a noticeable effect on the ratio $\xi_{\psi 2}/\xi_{\psi 1}$ due to the active feedback, but it is greatly reduced from that of the $\kappa = 2.5$ and $\kappa = 3$ equilibria. Finally, the $\kappa = 1.75$ case shows an even smaller modification of the eigenfunction than the $\kappa = 2$ case with the ratio $\xi_{\psi 2}/\xi_{\psi 1}$ never being greater than 0.5. It is clear that the deformation due to the active feedback is strongly increasing with elongation, even for these cases in which the passive growth rate is the same.

Figure 11b shows the variation in the ratio $\xi_{\psi 3}/\xi_{\psi 1}$ for these same cases. For the $\kappa = 3$

case there is a strong deformation of the $m = 3$ component as well, which approaches 90% of the $m = 1$ component at the edge for the highest feedback gains. The effect of this active feedback configuration on the $m = 3$ component is much weaker for the equilibria of lower elongation. For the $\kappa = 2.5$ case the ratio $\xi_{\psi 3}/\xi_{\psi 1}$ increases only slightly with increasing feedback. For the $\kappa = 2$ case there is a very slight decrease, but hardly any change due to the feedback. For $\kappa = 1.75$ there is a slightly larger, but still very small, decrease in the value of $\xi_{\psi 3}/\xi_{\psi 1}$.

We can get a better idea of the deformation by looking at the perturbed flux contour plots. Figure 12 shows the plots of perturbed flux for three equilibria of different shapes ($\kappa = 2.0,\ 2.5,\ 3.0$) at the marginal stability points of the corresponding three curves of Fig. 11. It is useful to compare these plots to those shown in Fig. 13 for the same three equilibria, but without any active feedback.

In Fig. 12 we see how the perturbed flux contours of the plasma are strongly pushed towards the inboard side, corresponding to the strong variation in the $m = 2$ component seen in Fig. 11. The decrease in the magnitude of the deformation with decreasing elongation is clear. For the $\kappa = 3.0$ case, we see that the zero-flux contour (dotted) actually extends slightly inside the plasma. This means that there is a small region within the plasma (outside this contour) where the perturbed flux has reversed sign. The contours of perturbed flux inside the plasma are seen to be strongly deformed. At $\kappa = 2.5$ the deformation is reduced somewhat, with the zero-flux contour close to the plasma edge, but entirely outside. The deformation of the $\kappa = 2.0$ case is still noticeable, with the plasma contours shifted towards the inboard side, but they are not nearly as affected by the feedback as the more highly elongated cases.

4.2. *Active Feedback Induced $m = 3$ Deformation*

Now we alter the configuration slightly by adding a pair of coils on the inboard side at $X = 0.50$ m, at the same vertical position as the outboard pair. This is similar to the last case of Section 3.2.1 (see Figs. 6 and 7) in which we saw a very large deformation due to an enhancement of the $m = 3$ component by the feedback system. Therefore we will examine the variation of particularly the $m = 3$ component with increasing feedback using this configuration for the same four equilibria used above.

Figure 14a shows the variation of the ratio $\xi_{\psi 3}/\xi_{\psi 1}$ vs. the growth rate for the four equilibria of differing elongation as they are stabilized by the feedback system. For the $\kappa = 3$ case we see a very large deformation in the eigenfunction reflected by the enhancement of the $m = 3$ component which dominates the $m = 1$ component by almost a factor of 2 at the highest feedback. Again, the equilibria at lower elongation show a smaller deformation—much smaller in this case. Already, even at $\kappa = 2.5$ the eigenfunction is affected by the feedback to a much smaller degree; $\xi_{\psi 3}/\xi_{\psi 1}$ never exceeds 0.6. At an elongation of $\kappa = 2$ or smaller, the $m = 3$ harmonic is not strongly affected at all by the feedback.

Figure 14b shows how $\xi_{\psi 2}/\xi_{\psi 1}$ is affected by this feedback system. In this case we see a fairly significant effect on the $m = 2$ harmonic for the $\kappa = 3$ equilibrium, just as we saw a strong effect on the $m = 3$ harmonic for this equilibrium in the previous case. There seems to be a fairly strong coupling between these harmonics at high elongation. For the lower elongation equilibria, we do not see a strong effect on the $m = 2$ harmonic. There is some variation for the $\kappa = 2$ and $\kappa = 2.5$ equilibria, but $\xi_{\psi 2}/\xi_{\psi 1}$ never exceeds 0.35. And for the lowest elongation equilibrium there is very little effect.

Figure 15 shows the contours of perturbed flux in the same way as Fig. 12, but for the case with the inboard and outboard feedback coils. The deformation of the contours (compared to Fig. 13) is quite dramatic for the $\kappa = 3$ case. The zero-flux contour extends inside the plasma boundary at the top and bottom, and the contours of perturbed flux

inside the plasma are squashed significantly. This corresponds to the large variation in the $m = 3$ component seen in Fig. 14. The deformation is considerably smaller in the $\kappa = 2.5$ case. The zero-flux contour remains outside the plasma, and the internal flux contours are not nearly as deformed as in the $\kappa = 3$ case. Finally, the $\kappa = 2$ case is relatively unaffected by the feedback.

5. Summary

We have shown that the eigenfunction of the axisymmetric mode of highly elongated plasmas is strongly affected by the active feedback system, and that variations in the active coils used, and even in the weighting given to a fixed set of coils, can significantly change this effect. The deformation can alter the effectiveness of a set of magnetic measurements used, and it is helpful to understand this in order to choose an effective combination of magnetic measurements for the active feedback system of highly elongated plasmas. Measurements of the vertical displacement based on a single pair of flux loops were found to be ineffective in many cases. A combination of weighted flux measurements also failed in many cases. Combinations of flux loops and B_p-coils are more effective, but were also found to fail in some cases. However a measurement of vertical displacement that combines many poloidal flux and magnetic field measurements, plus corrections due to vessel eddy currents and active feedback coil currents was found to be effective in all cases—including those with the largest deformations of the eigenfunction. Therefore active feedback induced deformations should not have a detrimental effect on the TCV vertical feedback control.

We have also shown that the amount of deformation is a strong function of the elongation of the equilibrium. For a case using a pair of outboard coils, there is a strong enhancement of the $m = 2$ harmonic of the eigenfunction for equilibria with elongation greater than $\kappa = 2$. This enhancement becomes larger as the elongation is increased. It is such that the $m = 2$ harmonic dominates $m = 1$ at the plasma edge by a factor of two at the largest

feedback gains. There is some coupling to, and enhancement of, the $m = 3$ harmonic, but this is significant only for the most highly elongated ($\kappa = 3$) equilibrium.

For the case using also a pair of inboard coils, there is a strong enhancement of the $m = 3$ harmonic for the $\kappa = 3$ case. At lower elongations the deformation is much less significant. There is also a coupling to, and enhancement of, the $m = 2$ component for this case, but this is again only large for the $\kappa = 3$ equilibrium. Since the degree of deformation is a strong function of elongation, it is likely to also be strongly affected by other shape parameters such as triangularity δ and squareness λ (see. Eq. (1)), however these dependences have not been explored here.

Acknowledgment

This work was supported in part by the Swiss National Science Foundation.

REFERENCES

[1] Troyon, F., Gruber, R., Saurenmann, H., et al., Plasma Phys. and Contr. Fusion **26** (1984) 209.

[2] Goldston, R. J., Plasma Phys. and Contr. Fusion **26** (1984) 87.

[3] Lazarus, E. A., Chu, M. S., Ferron, J. R., et al., Phys. Fluids **B3** (1991) 2220.

[4] Lazarus, E. A., Lister, J. B., Neilson, G .H., Nucl. Fusion, **30** (1990) 111.

[5] Lister, J. B., Lazarus, E. A., Kellman, A. G., et al., Nucl. Fusion **30** (1990) 2349.

[6] Perrone, M. R., Wesson, J. A., Nucl. Fusion **21** (1981) 871.

[7] Pomphrey, N., Jardin, S. C., Ward, D. J., Nucl. Fusion **29** (1989) 465.

[8] Ward, D. J. and Jardin, S. C., Nucl. Fusion **32** (1992) 973.

[9] Hofmann, F., Jardin, S. C., Marcus, F. B, et al., in Fusion Technology (Proc. 14th Symp. Avignon, 1986), Vol. 1, Pergamon Press, Oxford (1986) 687.

[10] Ward, D. J., Jardin, S. C., and Cheng, C. Z., J. Comput. Phys. **104** (1993) 221.

[11] Eriksson, G., Bondeson, A., Ward, D. J., et al., in 1992 International Conference on Plasma Physics (Proc. 9th Conf. Innsbruck, 1992), Vol. 16C, Part I, European Physical Society (1992) 343.

[12] Marcus, F. B., Hofmann, F., Jardin, S. C., et al., Nucl. Fusion **30** (1990) 1511.

[13] Hofmann, F. and Jardin, S. C., Nucl. Fusion **30** (1990) 2013.

Figures

Fig. 1. TCV configuration showing plasma, vacuum vessel, internal and external active feedback coils, flux-loop detectors (marked by an 'X'), B_p-coils (marked by a 'c'), and the contours of perturbed plasma flux for the passive case with no active feedback.

Fig. 2. (a) Zero-flux contours for three different values of gain (dot-dash, dashed, dotted, respectively, with increasing gain) for the flux loops located at $(X, Z) = (0.60, \pm 0.772)$.
(b) Zero-flux contours for three different values of gain for the flux loops located at $(X, Z) = (0.584, \pm 0.690)$.

Fig. 3. (a) Evolution of the components of the eigenfunction $\xi_{\psi m}/\xi_{\psi 1}$ with respect to gain for the case with the flux loops loops located at $(X, Z) = (0.60, \pm 0.772)$. The perturbed flux signal $\delta\chi$ measured at the flux loops is also shown.
(b) Variation of the $m = 2$ component, $\xi_{\psi 2}/\xi_{\psi 1}$, and of the growth rate, γ, with respect to gain.

Fig. 4. (a) Evolution of the components of the eigenfunction $\xi_{\psi m}/\xi_{\psi 1}$ with respect to gain for the case with the flux loops loops located at $(X, Z) = (0.584, \pm 0.690)$. The perturbed flux signal $\delta\chi$ measured at the flux loops is also shown.
(b) Variation of the $m = 2$ component, $\xi_{\psi 2}/\xi_{\psi 1}$, and of the growth rate, γ, with respect to gain.

Fig. 5. Complete set of perturbed flux contours for the case with the flux loops located at $(X, Z) = (0.584, \pm 0.690)$ with the gain that of the marginal stability point of Fig. 4. The zero-flux contour is the dotted curve.

Fig. 6. (a) Evolution of the components of the eigenfunction $\xi_{\psi m}/\xi_{\psi 1}$ with respect to gain for the case using the internal feedback coils and one pair of inboard, external coils.
(b) Variation of the $m = 3$ component, $\xi_{\psi 3}/\xi_{\psi 1}$, and of the growth rate, γ, with respect to normalized gain.

Fig. 7. Perturbed flux contours for the case using the internal feedback coils, and one pair of inboard, external coils. The zero-flux contour is the dotted curve.

Fig. 8. Perturbed flux contours for the case using the internal coils and all external coils with equal weighting. The zero-flux contour is the dotted curve.

Fig. 9. (a) Evolution of the components of the eigenfunction $\xi_{\psi m}/\xi_{\psi 1}$ with respect to normalized gain for the case using the internal feedback coils, weighted external coils, and the full detection system described in Eq. (8). The normalized, corrected, measured signal $|\delta Z|$ is also shown with respect to the gain. (b) Variation of the $m = 2$ component, $\xi_{\psi 2}/\xi_{\psi 1}$, and the growth rate, γ, with respect to the normalized gain.

Fig. 10. Perturbed flux contours for the case with internal coils and weighted external coils.

Fig. 11. (a) Variation of the ratio $\xi_{\psi 2}/\xi_{\psi 1}$ vs. growth rate for four equilibria of different elongation for the case using two feedback coils on the outboard side.
(b) Variation of the ratio $\xi_{\psi 3}/\xi_{\psi 1}$ vs. growth rate for the same four equilibria.

Fig. 12. Perturbed flux contours for the equilibria of differing shape: (a) $\kappa = 3.0$, (b) $\kappa = 2.5$, (c) $\kappa = 2.0$, for the case with active feedback by a single pair of active coils on the outboard side. The contour of zero flux is the dotted curve.

Fig. 13. Perturbed flux contours for the equilibria of differing shape: (a) $\kappa = 3.0$, (b) $\kappa = 2.5$, (c) $\kappa = 2.0$, for the case with no active feedback.

Fig. 14. (a) Variation of the ratio $\xi_{\psi 3}/\xi_{\psi 1}$ vs. growth rate for the case using two outboard and two inboard coils for the four equilibria of differing elongation.
(b) Variation of the ratio $\xi_{\psi 2}/\xi_{\psi 1}$ vs. growth rate for the same equilibria.

Fig. 15. Perturbed flux contours for the equilibria of differing shape: (a) $\kappa = 3.0$, (b) $\kappa = 2.5$, (c) $\kappa = 2.0$, for the case with active feedback by a pair of active coils on the inboard side and a pair on the outboard side. The contour of zero flux is the dotted curve.

Figure 1

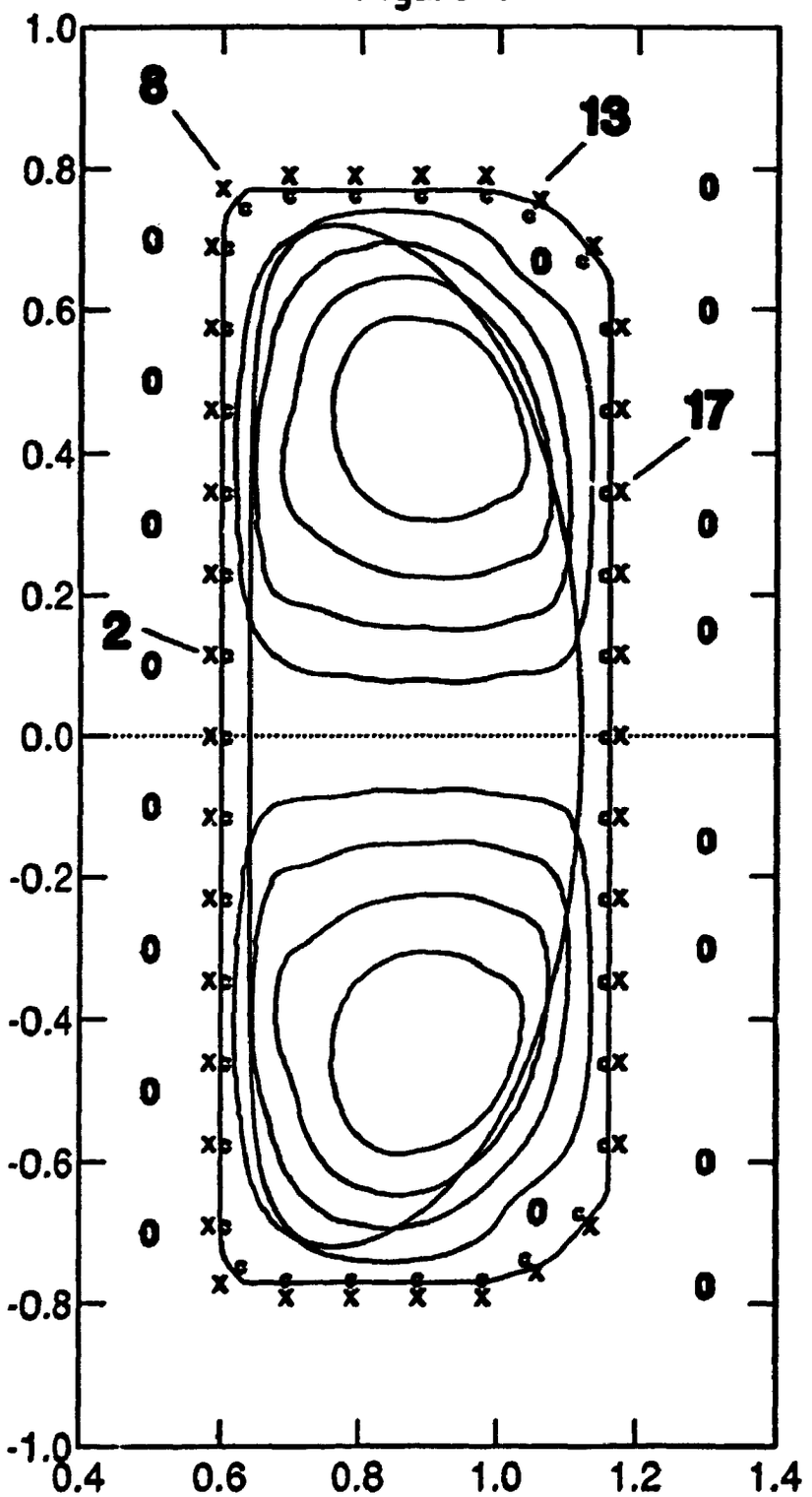

Figure 2a

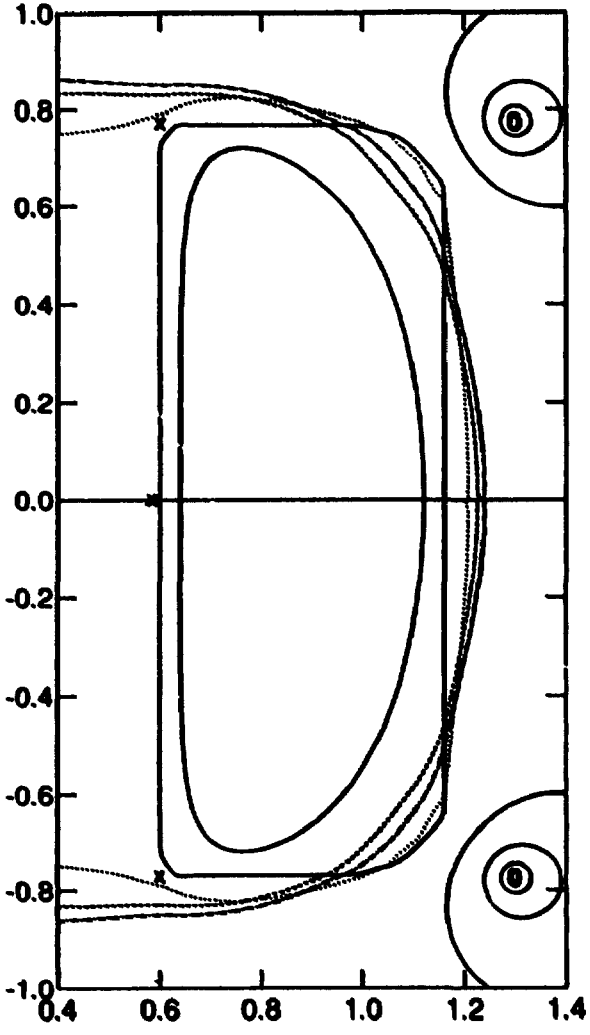

Figure 2b

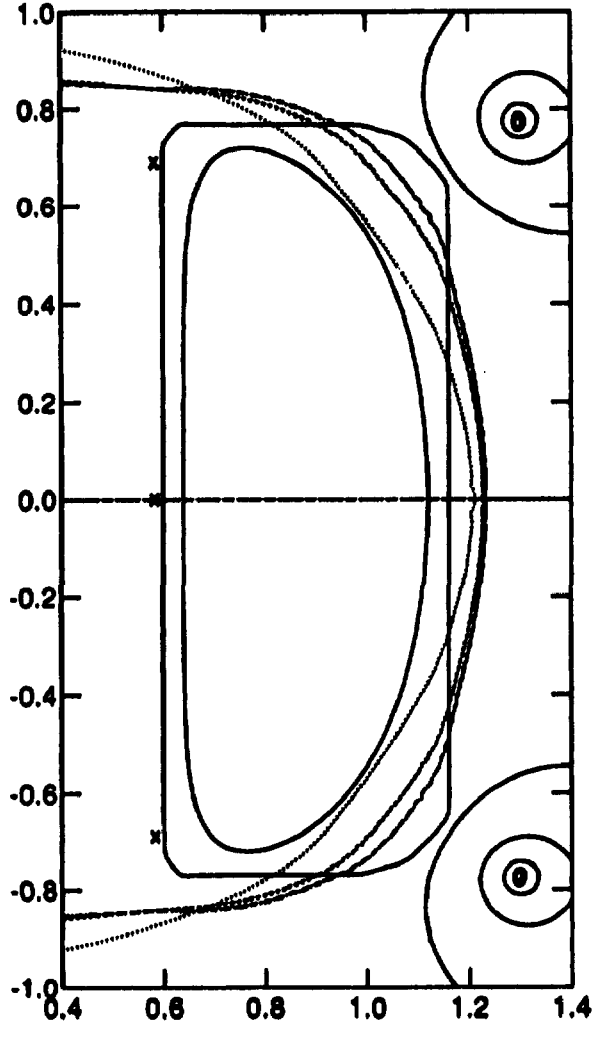

Figure 3a

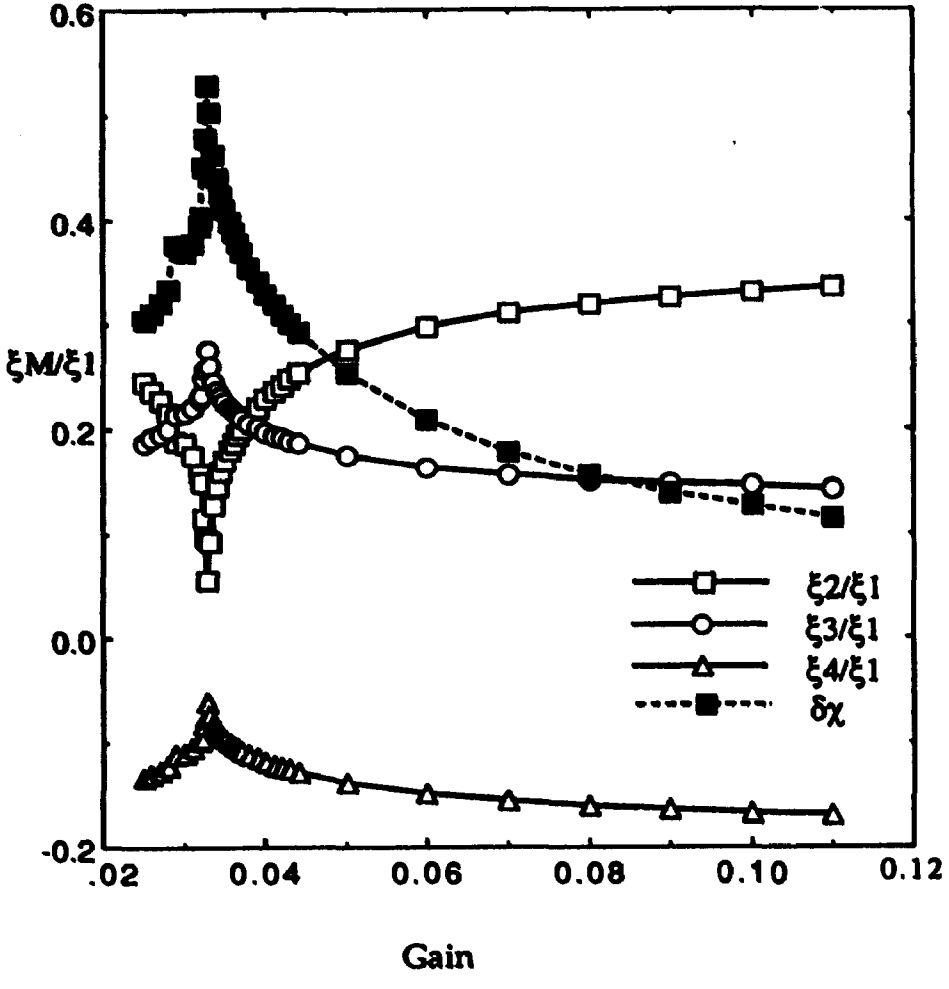

Figure 3b

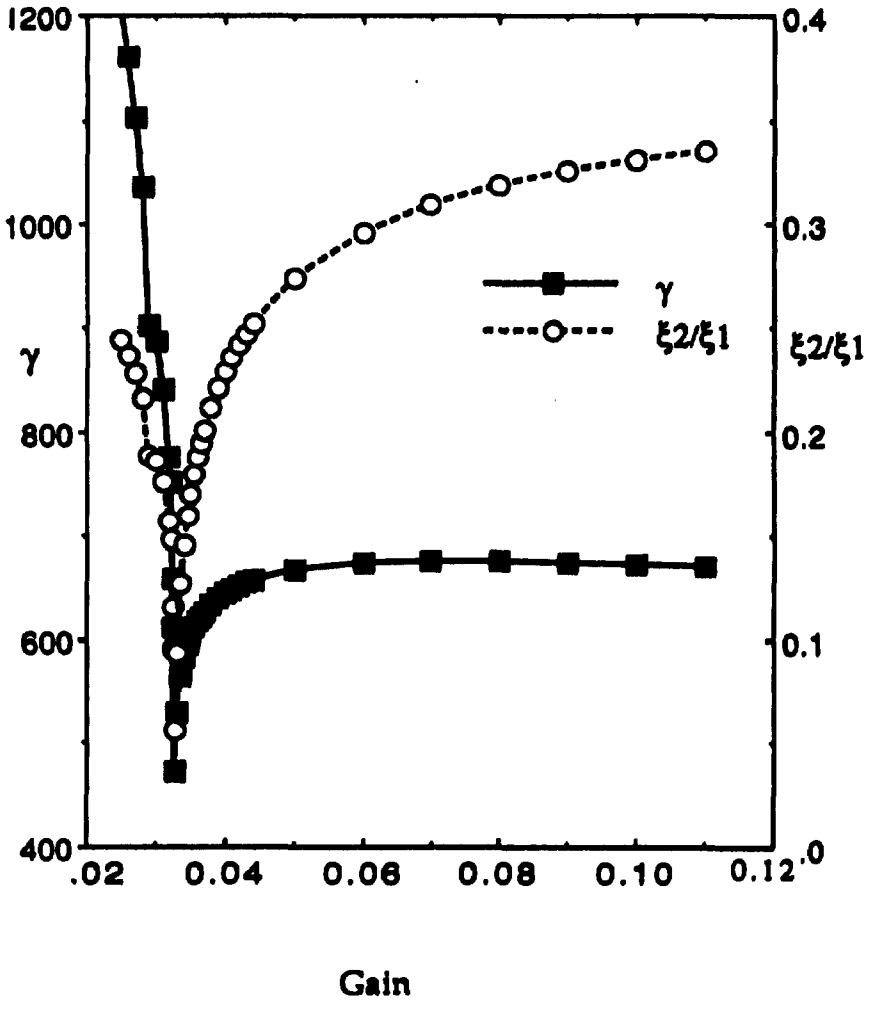

Figure 4a

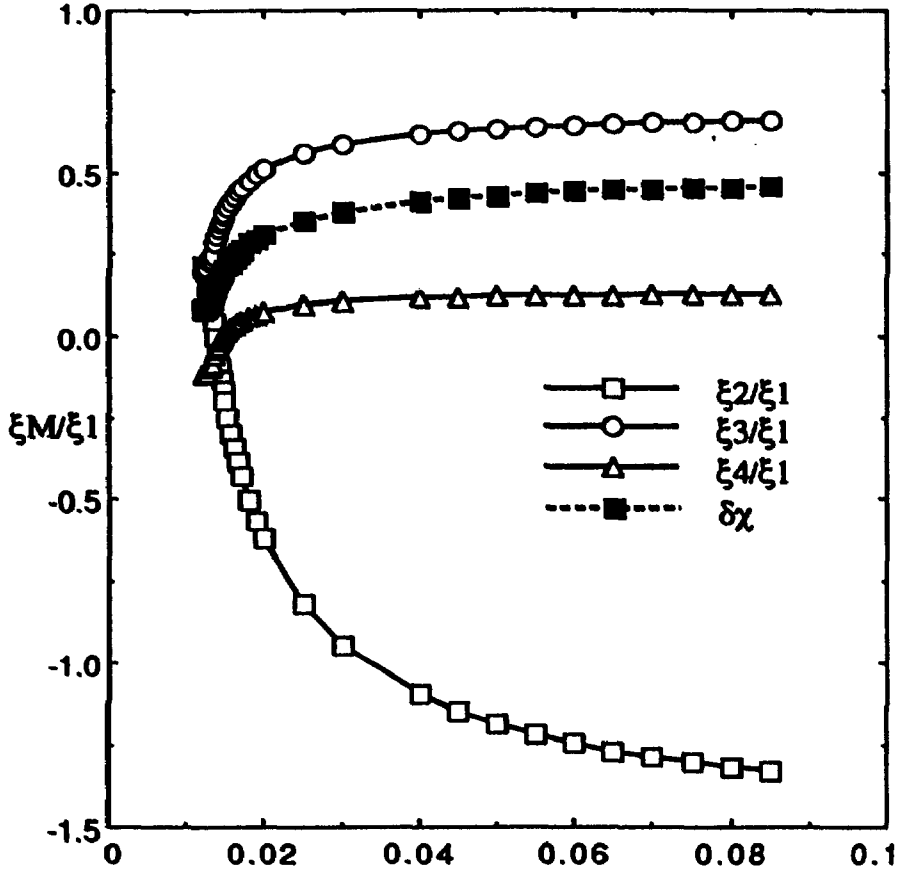

Gain

Figure 4b

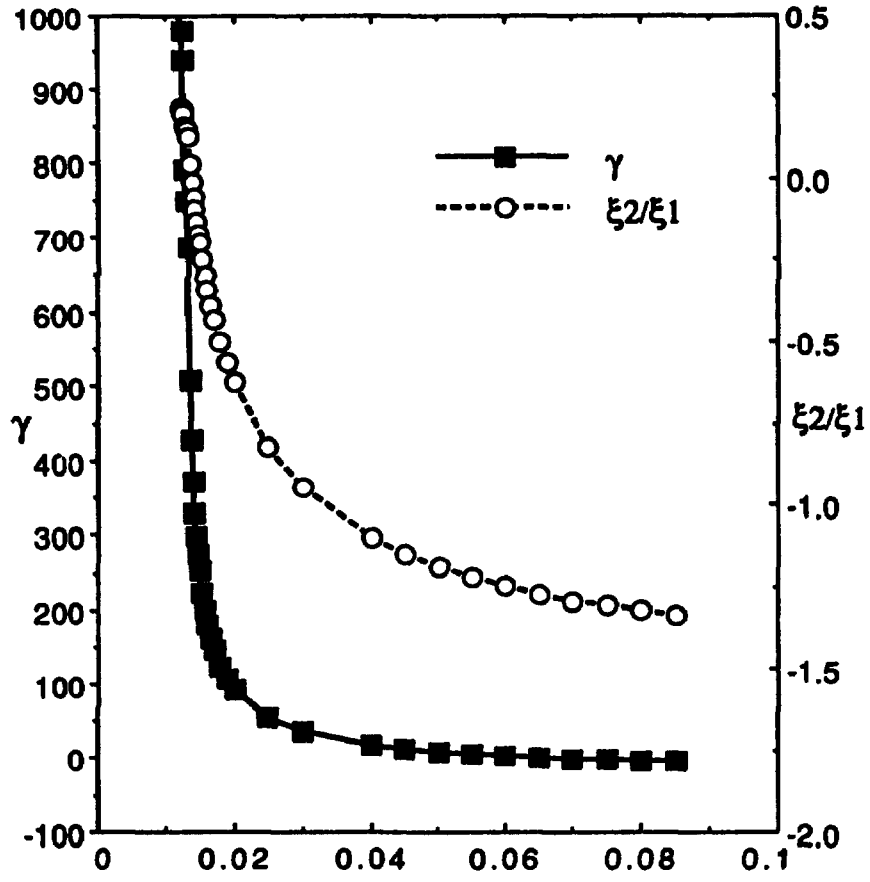

Gain

Figure 5

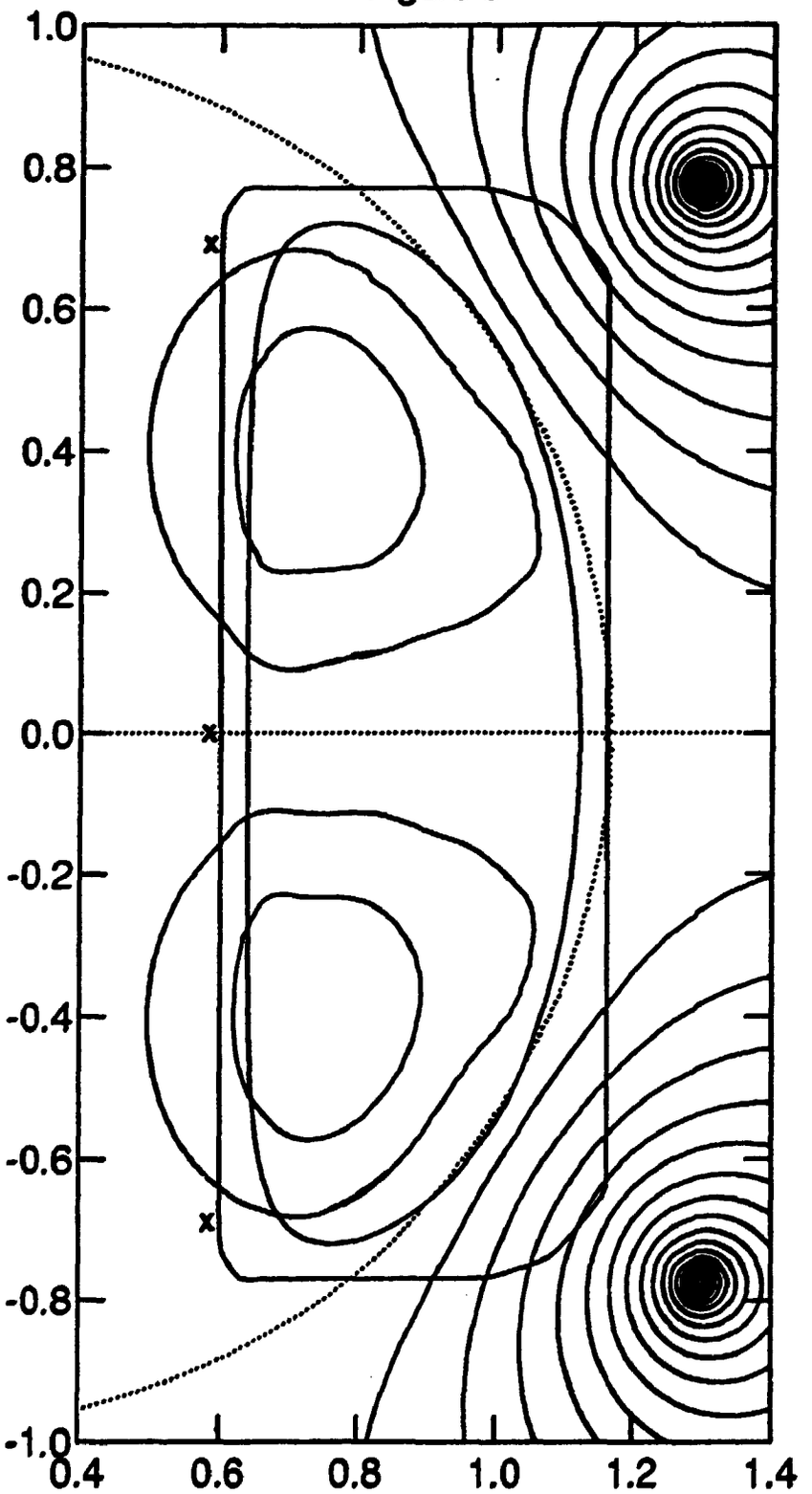

Figure 6a

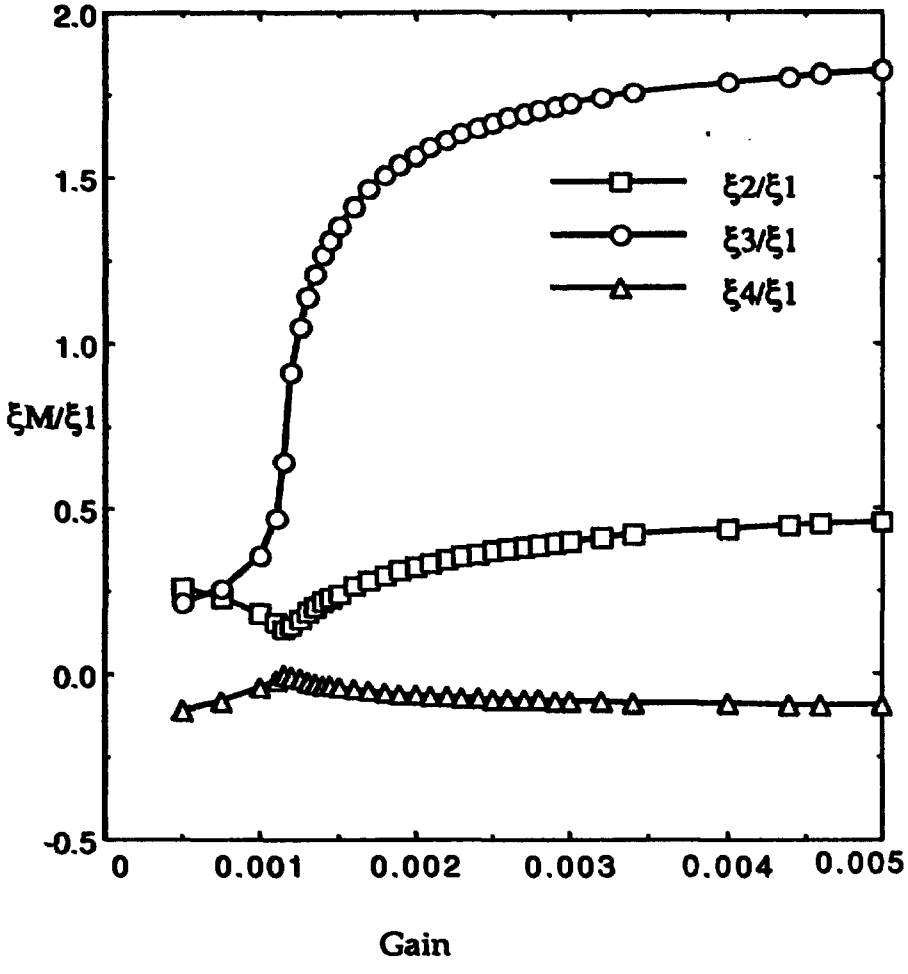

Figure 6b

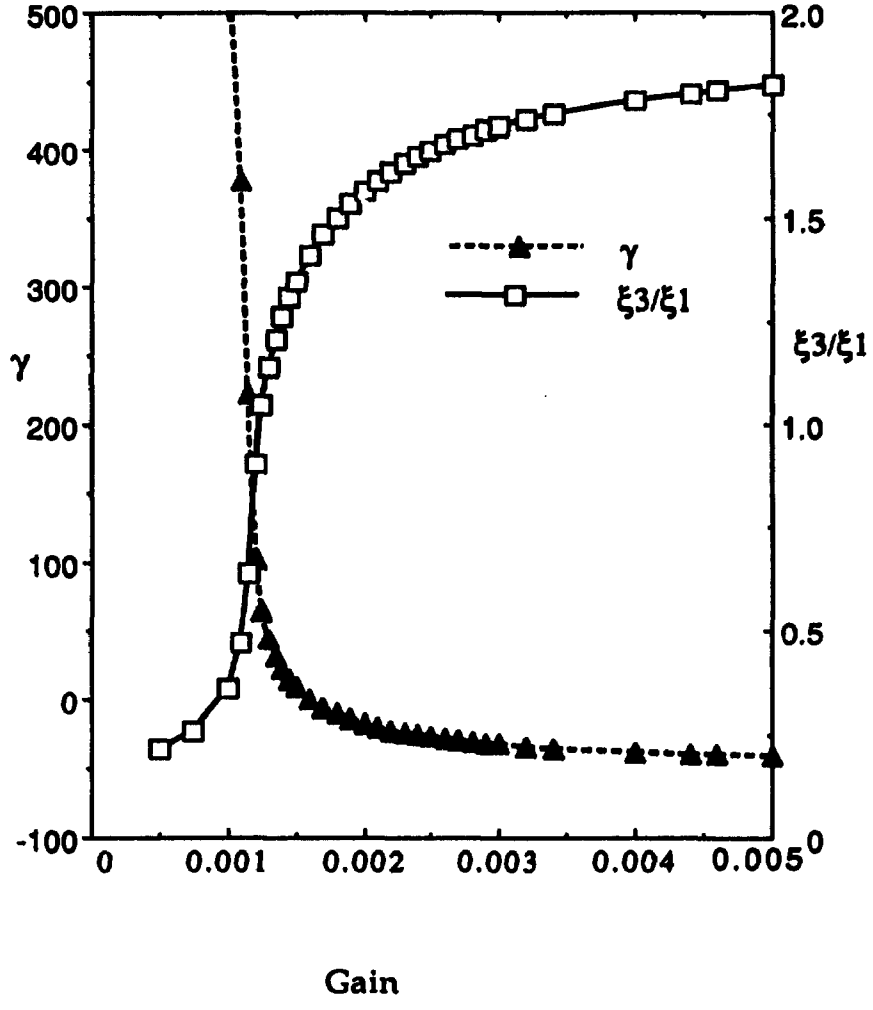

Figure 7

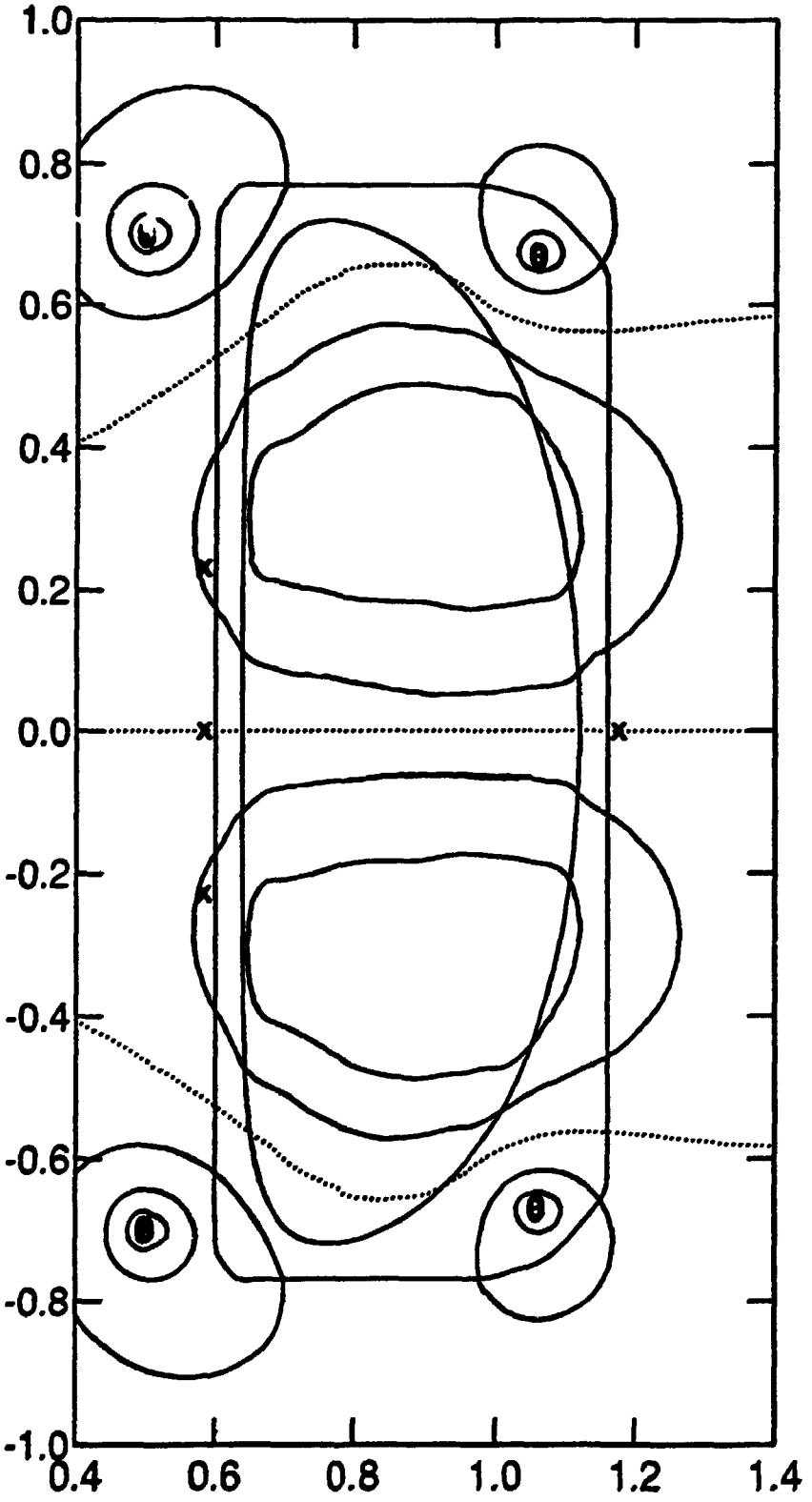

Figure 8

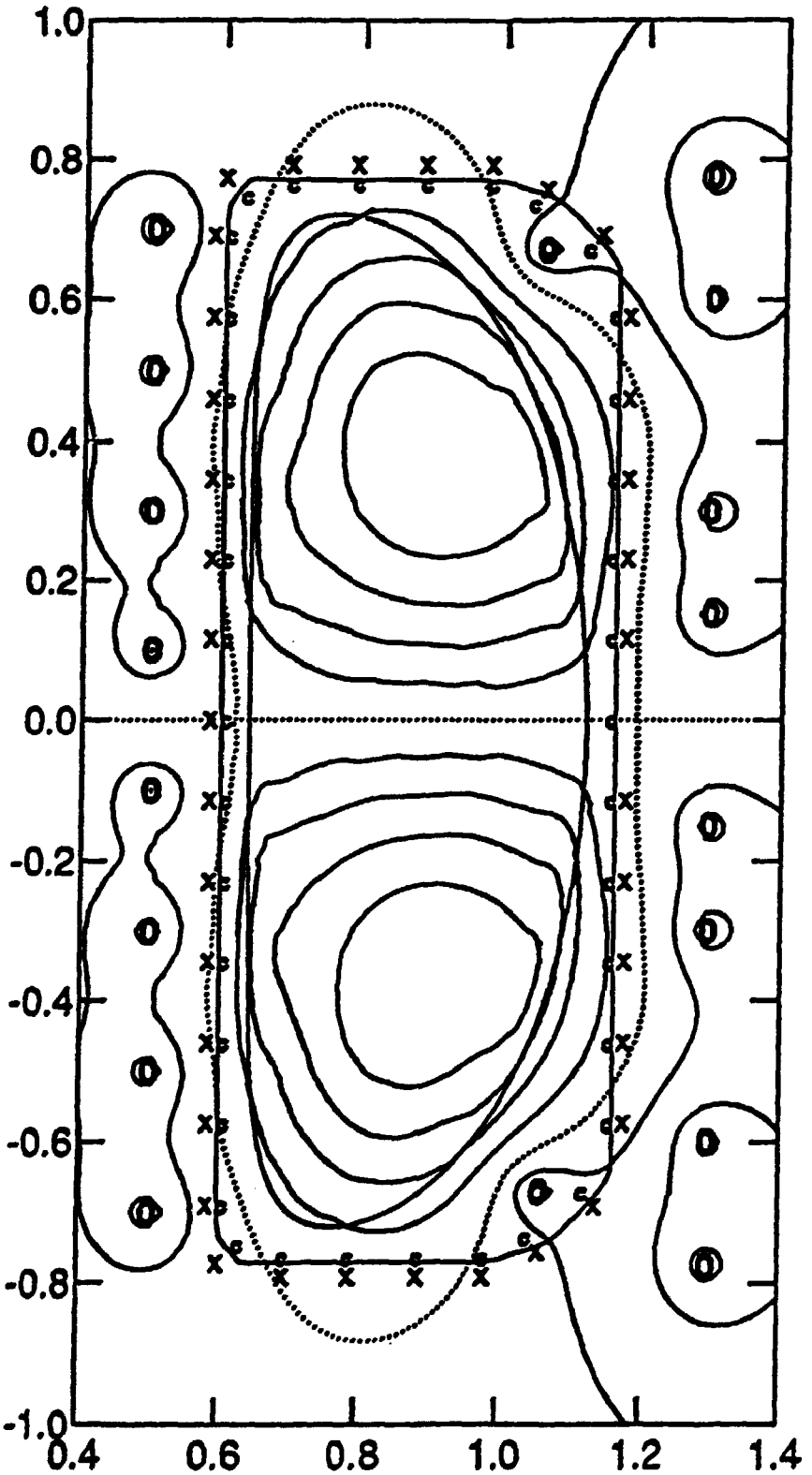

Figure 9a

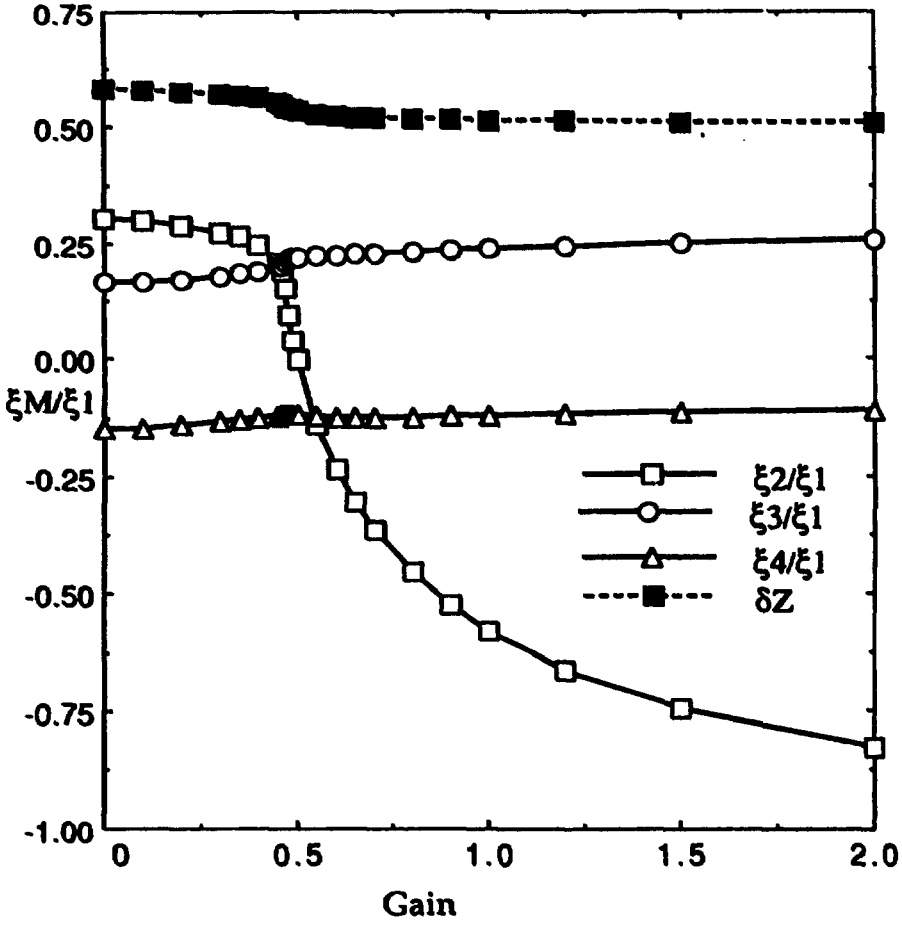

Figure 9b

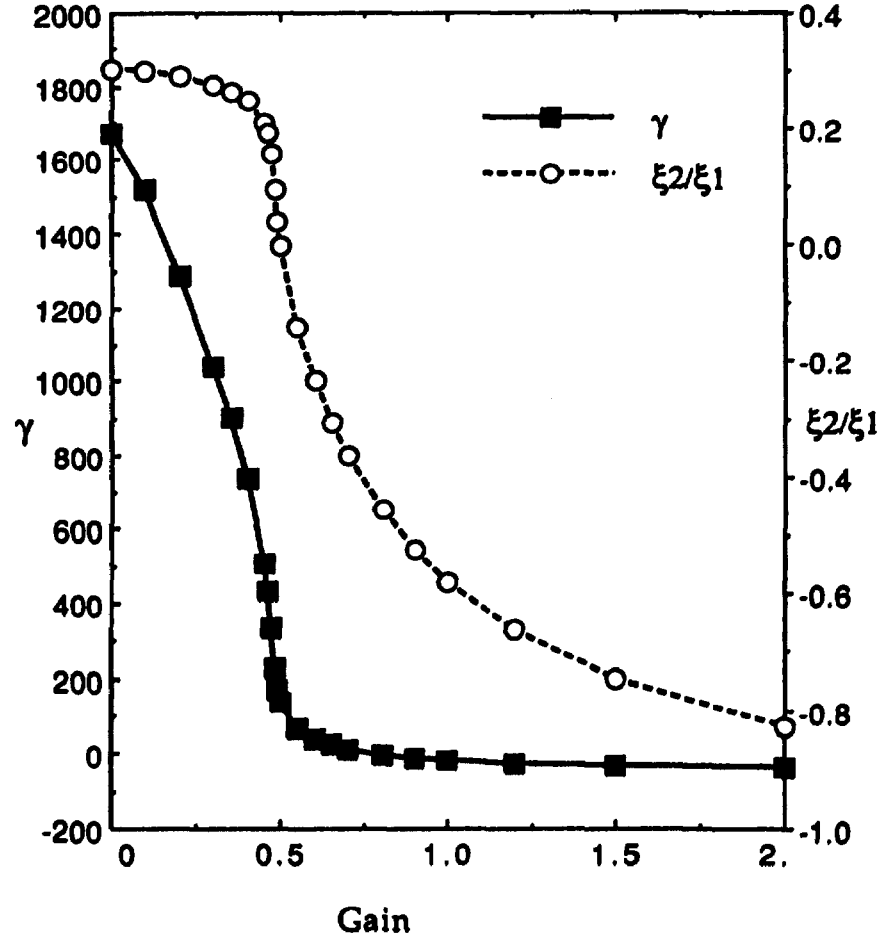

Figure 10

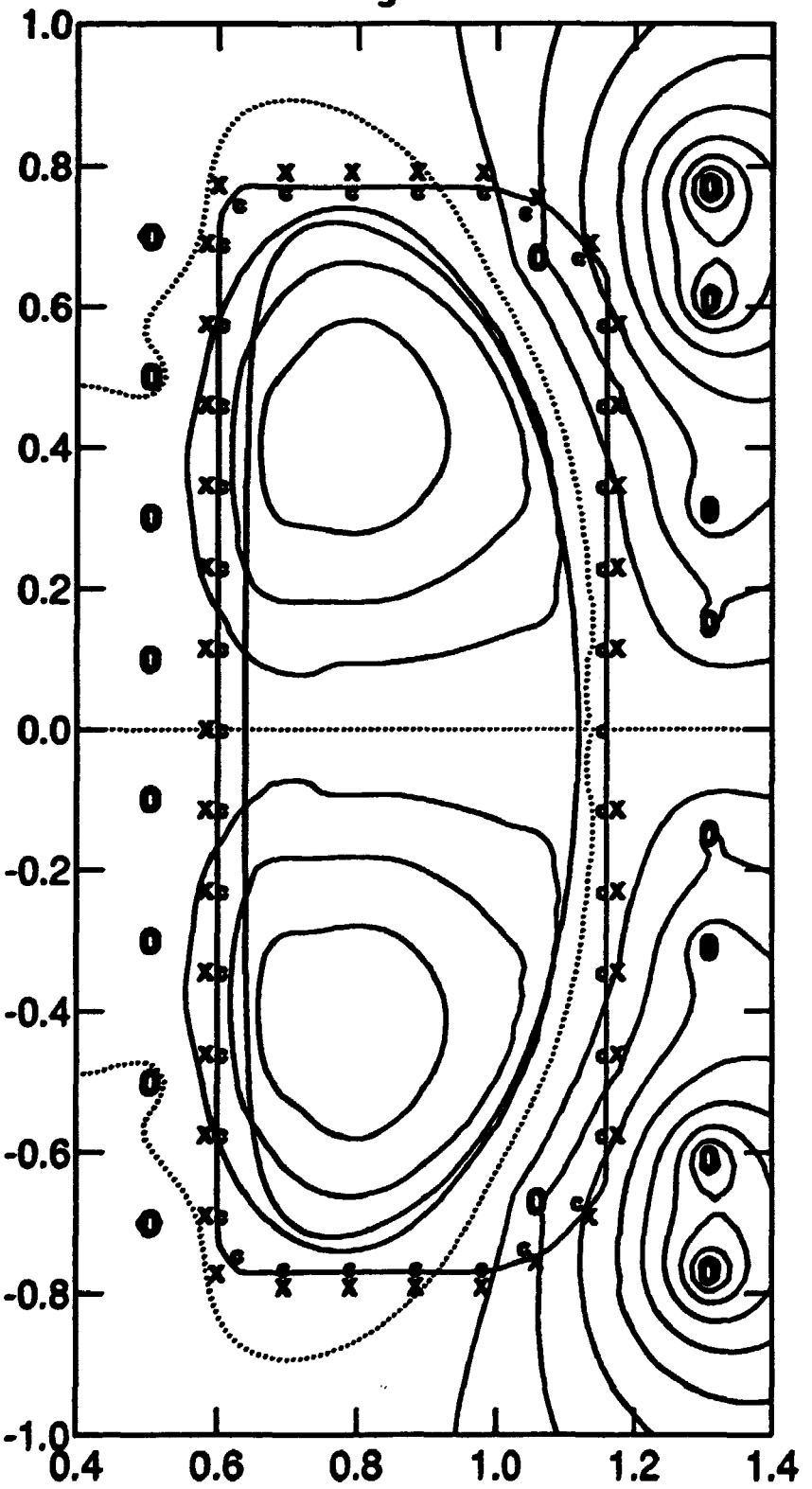

Figure 11a

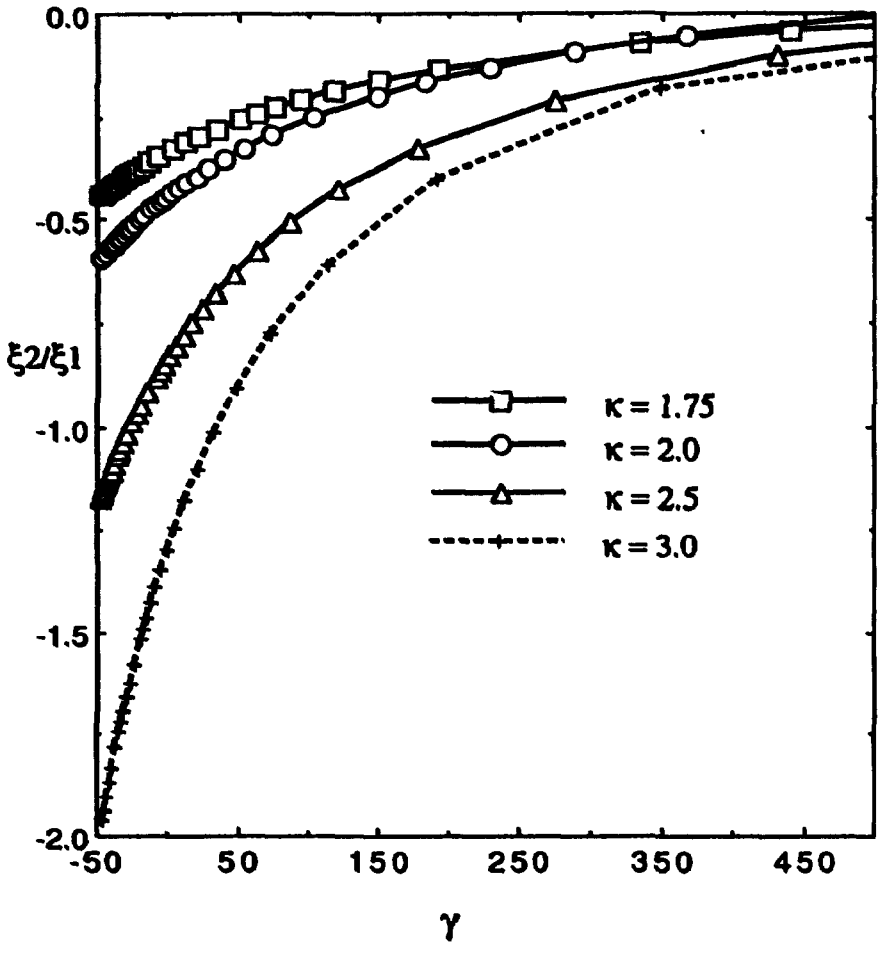

Figure 11b

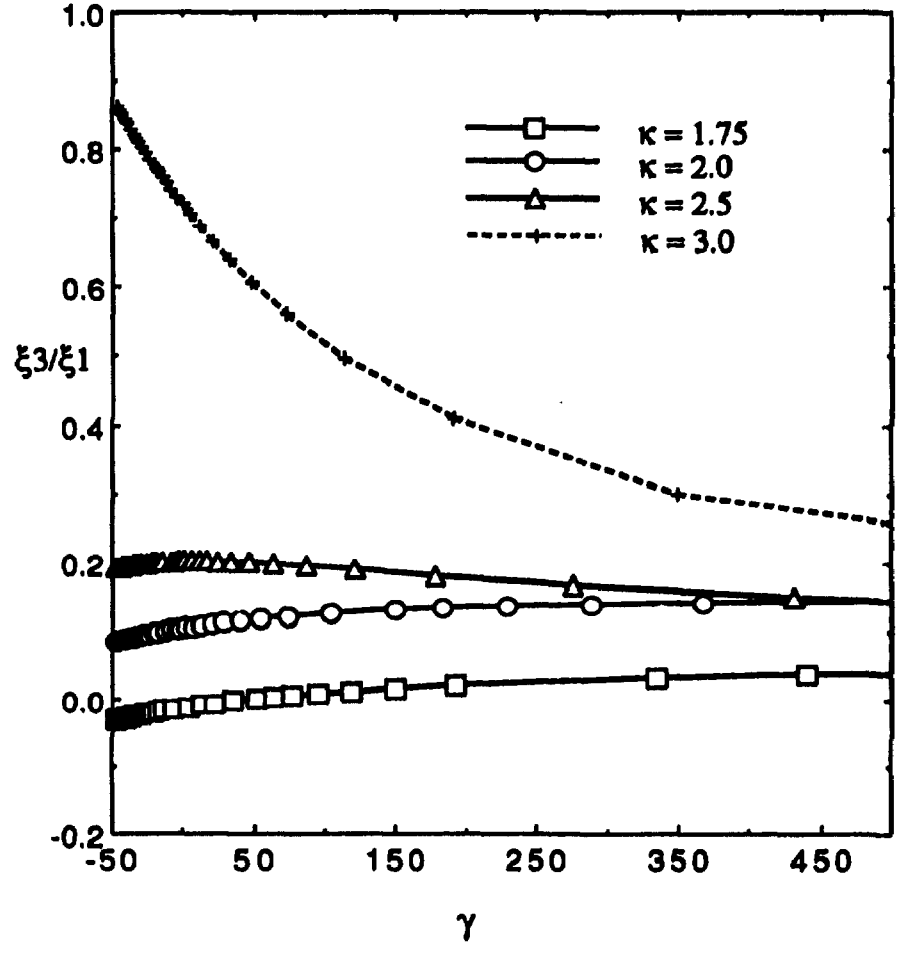

Figure 12a

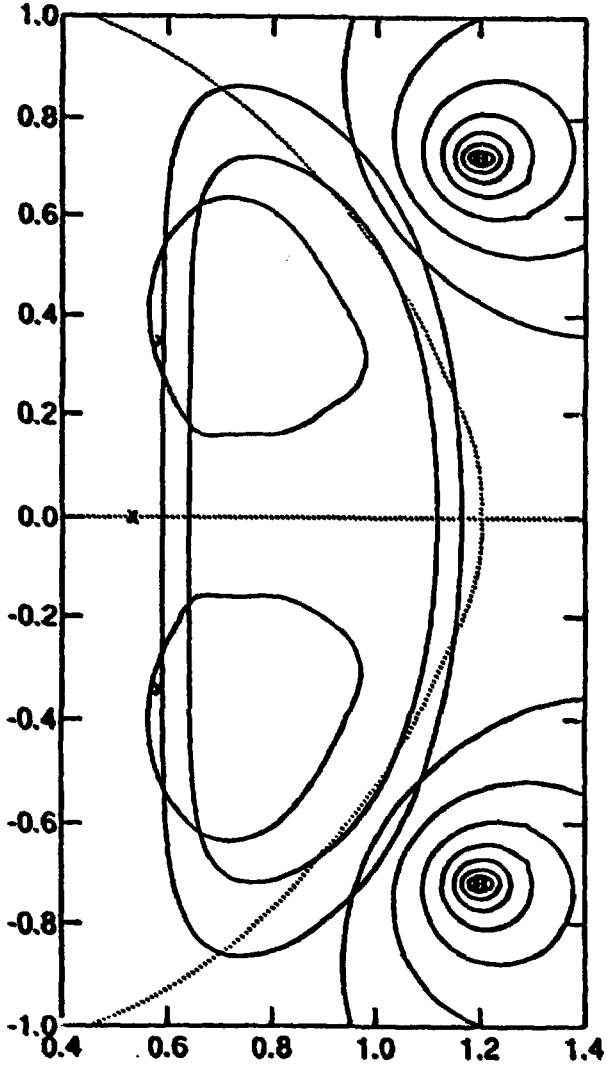

Figure 12b

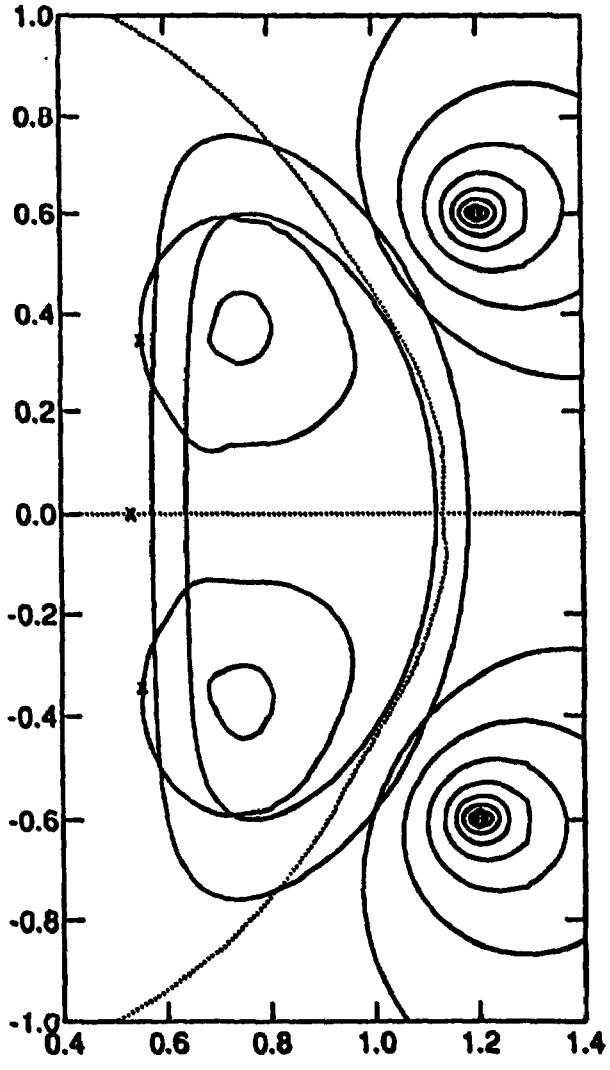

Figure 12c

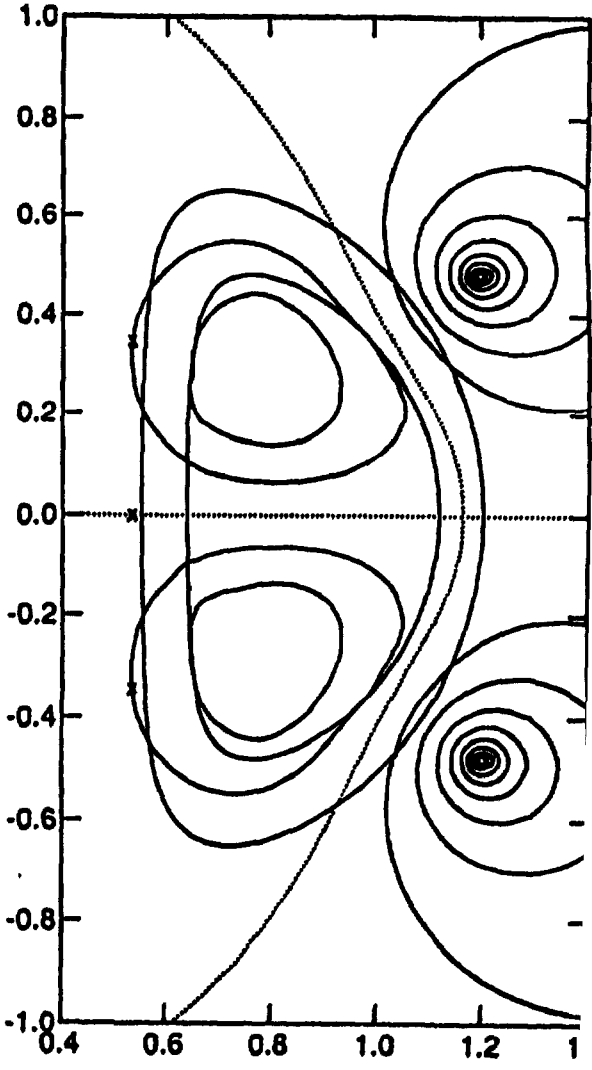

Figure 13a

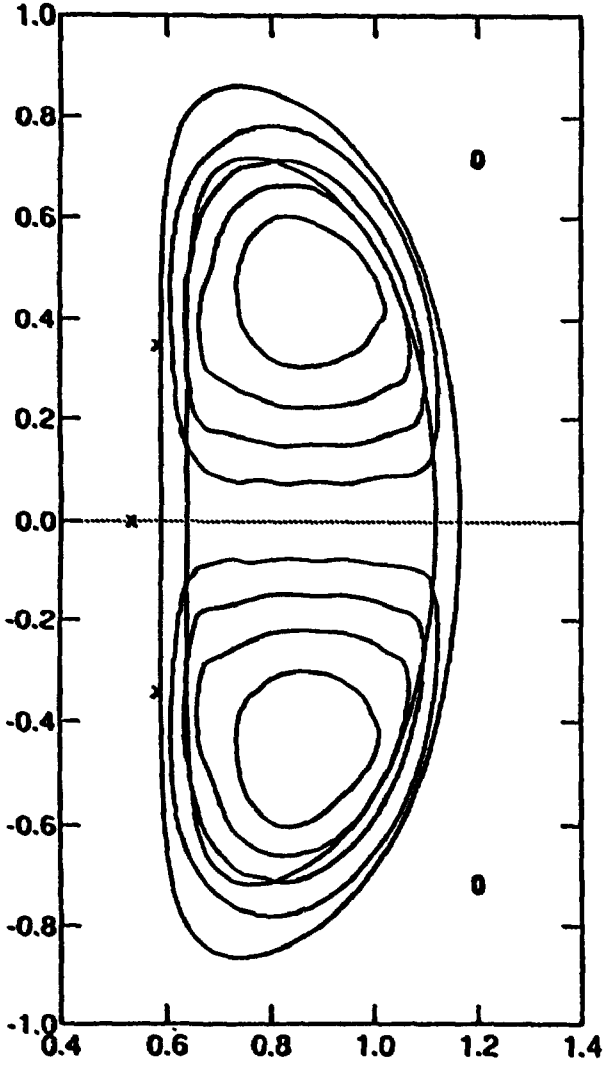

Figure 13b

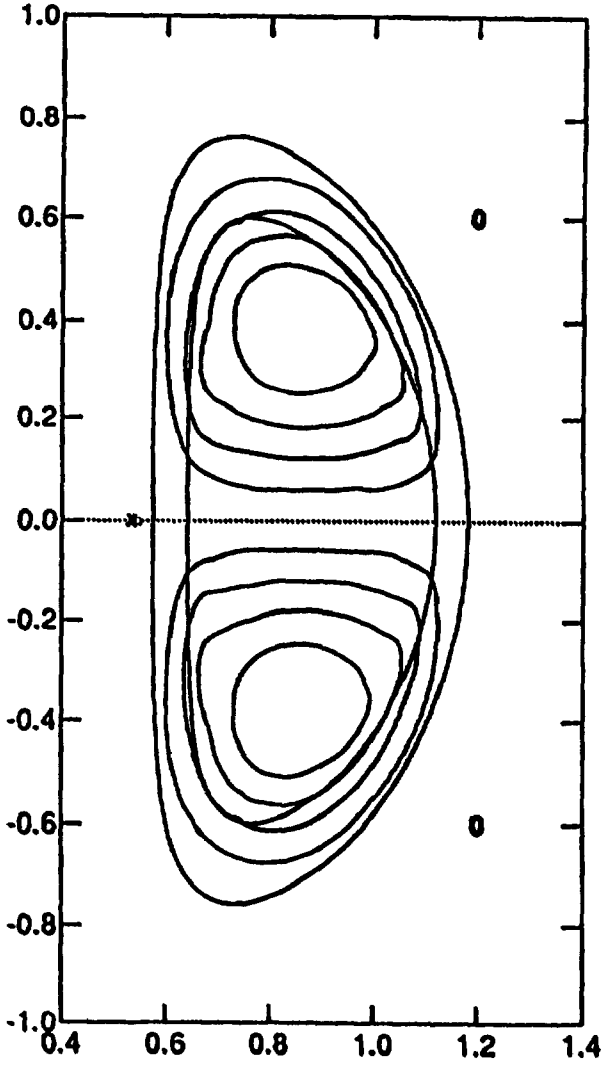

Figure 13c

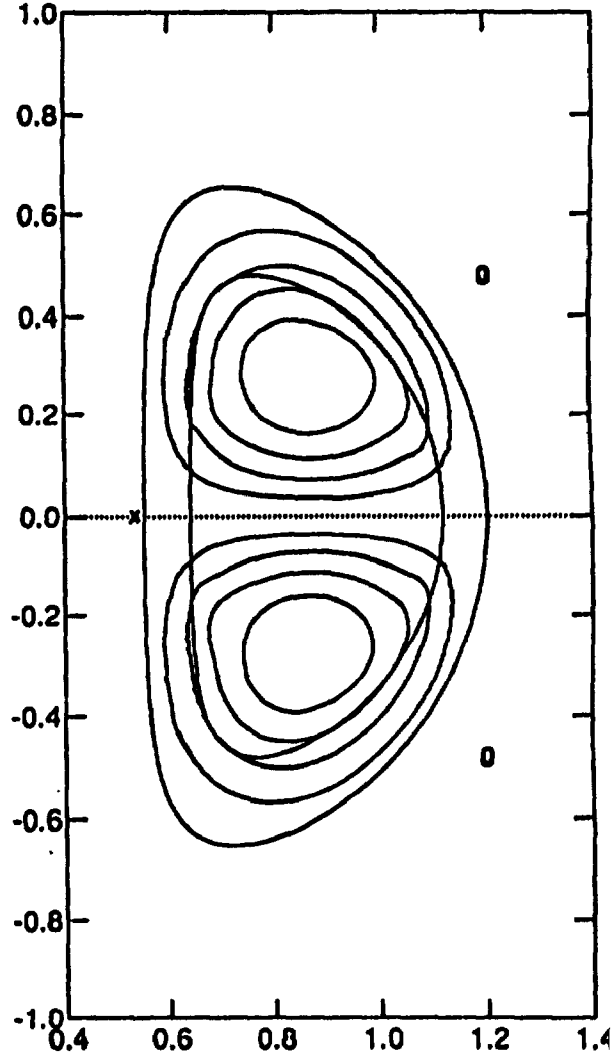

Figure 14a

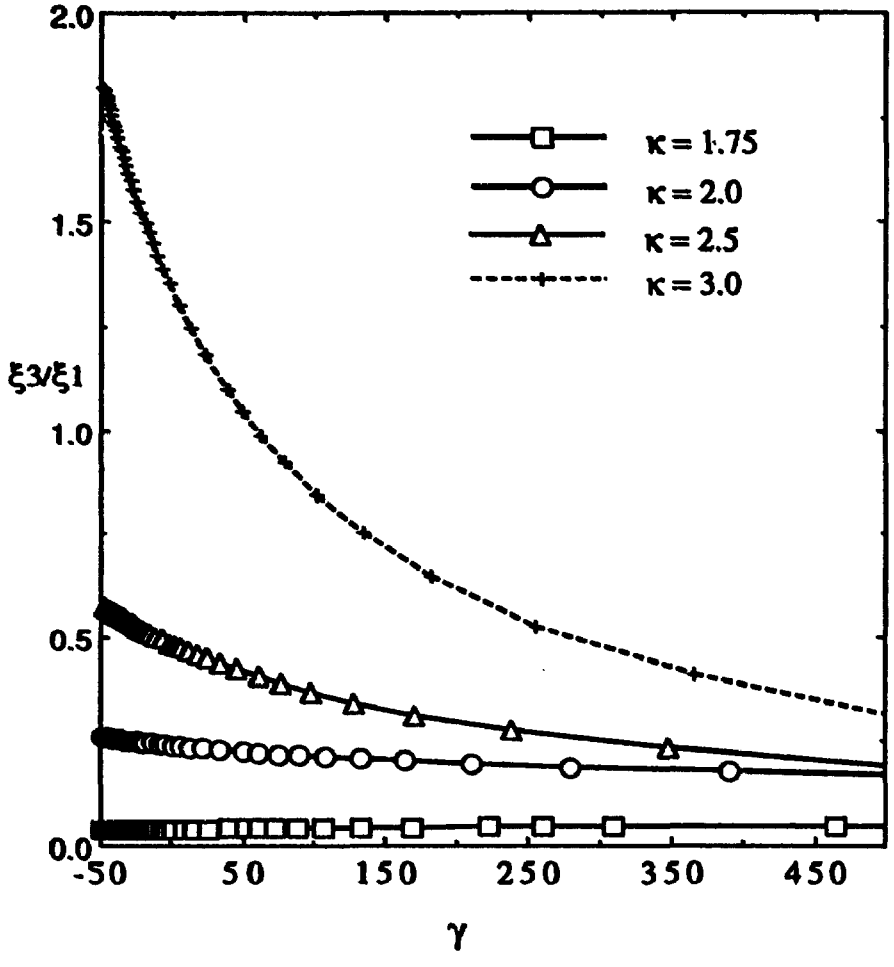

Figure 14b

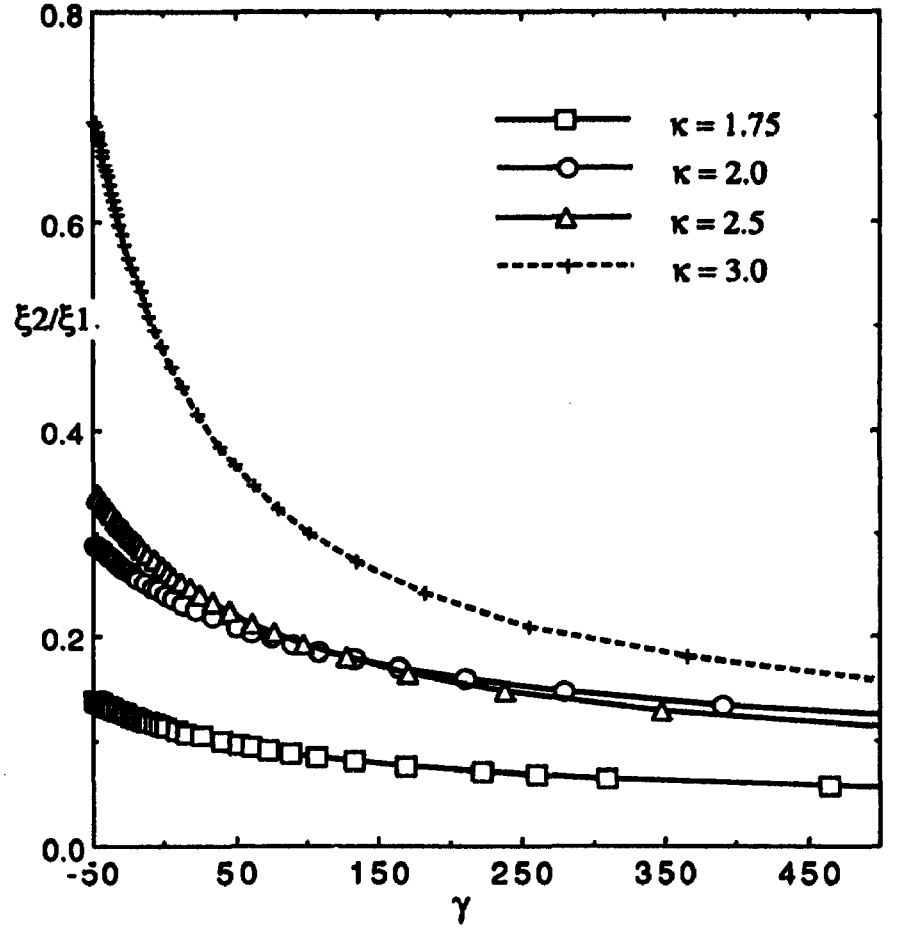

Figure 15a

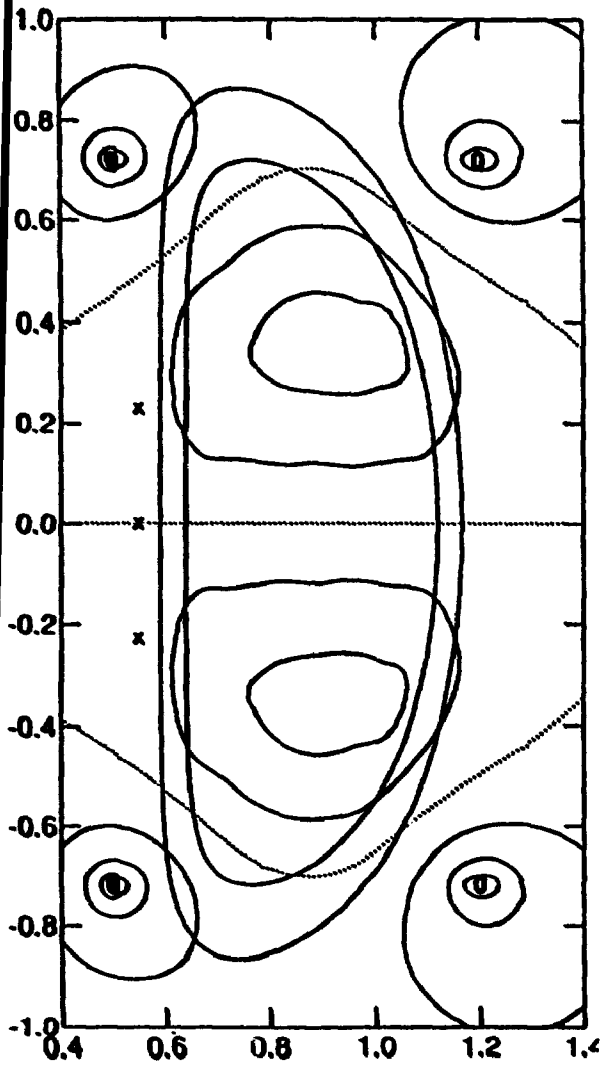

Figure 15b

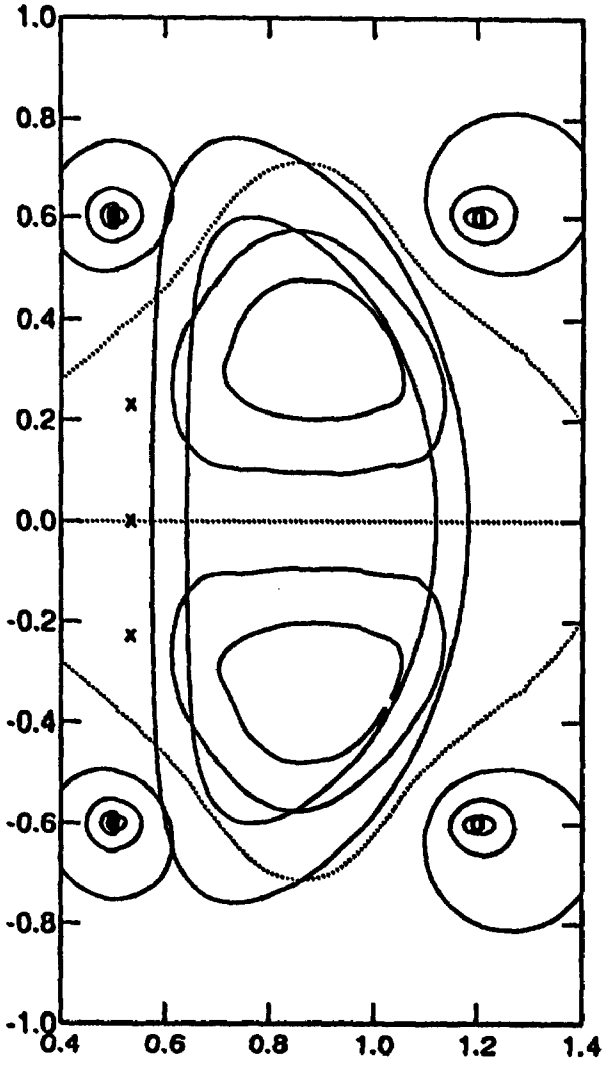

Figure 15c